공학박사학위논문

Development of Cell- and Protein-based Optical Methods of Odorant Detection for Visualization of Smell

냄새의 시각화를 위한 세포 및 단백질 기반의 광학적 냄새분자 측정 방법 개발

2014년 8월

서울대학교 대학원

공과대학 협동과정 생물화학공학

오 은 해

Abstract

Development of Cell- and Protein-based Optical Methods of Odorant Detection for Visualization of Smell

Eun Hae Oh
School of Biological and Chemical Engineering
The Graduate School
Seoul National University

Human olfactory system can detect and discriminate numerous odorant molecules with high sensitivity and selectivity using olfactory receptor (OR). Human has about 390 ORs and each OR can bind to various odorant with different affinity and one odorant molecule can also bind to various ORs. The smell is recognized through the various combination of bindings between OR and odorants. Many researchers have developed highly efficient odorant detection system by mimicking natural olfactory system. The artificial olfactory cells or OR protein have been used as a sensing material. However, up to now, only few ORs have been characterized because of the lack of effective screening tool. Thus the characterization of many orphaned ORs via new high-throughput system and the pattern analysis of odorant responses are inevitable for further applications of ORs.

In this thesis, the function of ORs and their response patterns in the presence of various compounds were analyzed visually via various optical analysis

systems. Using ORs and artificial olfactory cells as sensing material, the odorant binding event or the cellular response upon odorant stimulation was detected and visualized. The ORs, which were expressed in *E. coli* system with large quantity, were used as effective sensing materials in surface plasmon resonance (SPR)-based system after the purification and refolding steps. And for the high-throughput screening and visualization of various odorant responses, the artificial olfactory cells were used as sensing materials. The polyethlyenglycol (PEG) microwell was constructed as a miniaturized screening platform, and various ORs were expressed on the microwell using reverse transfection technique. The odorant response was visualized by CRE reporter assay system which expresses fluorescence protein as a reporter. The conventional odorant screening system has a limitation for high-throughput format because of the complicated experimental steps, while the PEG microwell-based system combined with a reverse transfection technique has advantages; various ORs can be expressed simultaneously and the imaging odorant response is stable and effective. However, this system requires a time for protein expression, thus a different approach to immediately detect and visualize the odorant response was also conducted.

For the real time detection and visualization of odorant response, ORs were linked to the potassium ion channel. The conformational change of OR by the odorant binding induces the ion channel physically opened. The odorant response was immediately visualized using membrane potential dye by detecting the potassium influx through the ion channel. In this study, various ORs were coupled to the ion channel for the visualization of various odorant

response patterns. The odorant detection using ion channel-coupled OR was majorly dependent on the conformational change of the physically linked-protein rather than intracellular transduction pathway. Based on this mechanism, it was demonstrated that the ion channel-coupled OR can be used as an effective protein-based odorant detection material for the real time visualization of odorant response.

Natural olfactory system detects the odorant in gaseous phase, thus, in this study, the detection of gaseous odorant is very important. In this study, the detection and visualization system of gaseous odorant was also developed using polycarbonate (PC) membrane and the microfluidic system. The OR-expressing cells were cultured on the PC membrane and placed in the PDMS chamber in the inverted format. Then the gaseous odorant was injected in the upper side of the chamber so that the cells could be exposed to the gas through the pores of the membrane. The odorant response was visualized using calcium imaging method.

The visualized odorant response can be used as a code for smell. The visualized patterns of smell can be used not only for understanding human olfactory system but also for various purposes in medical and industrial applications. This study offers various protein- and cell-based optical methods for the visualization of smell in high-throughput screening platform.

Keywords: visualization of smell, olfactory receptor, artificial olfactory cell, high-throughput screening system

Student number: 2005-20884

Contents

List of Figures

List of Abbreviations

ATP: adenosine tiphosphae

BRET: bioluminescence resonance energy transfer

cAMP: cyclic adenosine monophosphate

CNG: cyclic adeno monophosphate

CNT: carbon nanotube

CRE: cAMP response element

CREB: CRE binding protein

DD: destabilizing domain

DMEM: Dulbecco's modified Eagle's medium

DW: deionized water

E. coli: Escherichia coli

EC50: half maximal response

EGFP: enhanced green fluorescence protein

ELS: electrophoretic light scattering

FBS: fetal bovine serum

FET: field effect transistor

FRET: Fluorescence resonance energy transfer

FSK: forskolin

GPCR: G protein-coupled receptor

GST: glutathionse-S-tranferase

HEK-293: human embryonic kidney-293

IBMX: 3-isobutyl-1-methylxanthine

IP3: inositol (1, 4, 5) triphosphate

OR: olfactory receptor

OSN: olfactory sensory neuron

PBS: phosphate buffered saline

PC membrane: polycarbonate membrane

PCR: polymerase chain reaction

PDL: poly-D-lysine

PDMS: polydimethylsiloxane

PEGDA: polyethyleneglycol diacylate

PKA: protein kinase A

PS: penicillin-streptomysin

QCM: quartz crystal microbalance

RTP1S: receptor transfer protein 1

SPR: surface plasmon resonance

Chapter 1.

Research Background and Objective

Chapter 1. Research Background and Objective

Human olfaction perceives and discriminates thousands of odorant with high sensitivity and selectivity. The perception of smell is initiated by the binding of odorants to olfactory receptors (ORs)[1-4], which are expressed on the olfactory sensory neurons (OSNs). When the certain odorant binds to the specific OR, the intracellular signaling cascade is activated and produced the electrophysiological signal. The signal travels along the axons to the brain to recognize the smell. Human has about 390 different ORs and each OR binds to various odorants with different affinity and selectivity. The smell is recognized by the combination of the binding of each OR and odorant. Many researchers have conducted the various experiments to characterize the orphan ORs[5, 6]. However, most of human ORs are still orphan because of the labor-intensive and time-consuming experimental procedure for characterization of ORs.

Because of the high sensitivity and selectivity of OR, the cells expressing OR and the OR itself have been applied to construct odorant detection biosensor combining secondary transducer such as quartz crystal microbalance (QCM), SPR, microelectrode, field effect transistor (FET) for the industrial or medical applications. However, due to the lack of the database of odorant-OR binding, it is limited to only few odorant detection sensors. Thus, for the various application of odorant detection sensor, the database about various odorant-OR binding should be constructed by priority.

Moreover, since smell is recognized through the combination of the various odorants-OR binding, the pattern analysis of the odorant response is required. Although various well-plate-based odorant screening systems such as calcium imaging and CRE reporter system have been used to characterize the orphan ORs and to analyze the odorant binding pattern, it is difficult to characterize numerous ORs because of their time-consuming and labor-intensive experimental processes. The characterization of OR and pattern analysis can be accomplished more effectively if the odorant binding response can be visualized in a high-throughput system.

In this research, the optical detection methods of the odorant molecules for the visualization of odorant response were developed using the artificial olfactory cell and olfactory receptor protein. The SPR, fluorescence microscopy, fluorescence imaging system was applied to detect and visualized the odorant response of OR and the olfactory. The OR was expressed and purified in *E. coli* system with large quantity, and the reconstitution process was conducted to use the OR as a sensing material in SPR detection system. This system detected the specific odorant with high sensitivity and selectivity and also showed the purified and reconstituted OR from *E. coli* expression system can be used as an effective odorant detection material in the optical sensing system. Also, for the detection of various odorants with various ORs and the visualization of odorant binding response, poly ethylene glycol (PEG) microwell-based odorant detection system was developed. This system could visualize the odorant response of each OR simultaneously and showed the

possibility for a high-throughput odorants screening system and pattern analysis system. However, since the odorant response image is obtained by the expression of the fluorescence protein, it takes time to detect the odorant response. Thus, the real time visualization system of the odorant response was developed using the ion channel coupled-OR and membrane potential dye. Also, the visualization of gaseous odorant for the industrial application was conducted using microfluidic-based system.

In summary, the objectives of this study are:

1. Development of optical system for odorant detection using OR protein as a sensing material through the reconstitution process
2. Development of the PEG microwell-based odorant screening platform for the visualization of odorant response
3. Visualization and pattern analysis of odorant response in real time using ion channel-coupled OR
4. Combination of the artificial olfactory cell and the microfluidic system for the visualization of odorant response in gas phase

The visualization of odorant response of ORs could contribute to build database on the pattern analysis of various smells, and the visualized patterns can be used as code for smell.

Chapter 2.

Literature Review

Chapter 2. Literature Review

2.1 Olfaction

Olfaction is the most important sense for recognizing environmental conditions, such as looking for food, finding enemies, communicating with others, and interpreting their surroundings. Olfaction has evolved such that it can discriminate lots of odors even in very low concentration. Even humans, whose olfactory system has degenerated with the progress of civilization, can still detect some odors at concentrations as low as 10^{-3} ppb and discriminate 10,000 distinct odors[1, 7, 8]. Since Dr. Buck and Dr. Axel received the Novel prize for identifying the olfactory mechanism in 2004, many research groups, worldwide, have developed and studied artificial olfactory sensors due to its potential commercial applications. The electronic nose, which was made with chemical sensing material, was designed to mimic the mechanism of olfactory system to detect odorous chemicals[9-11]. However, this sensor had severe limitations due to its expensive cost, requirement of a large sample size for analysis and low sensitivity and specificity compared with an animals' olfactory system[12].

Cell- or protein-based olfactory biosensors have the potential to be used as effective tools to detect and discriminate lots of odorants with high sensitivity and selectivity[13, 14]. However, because the olfactory system consists of complex biochemical and electrophysiological processes, there have been many difficulties associated with developing this technology. Olfactory

biosensors can be divided into cell-based or protein-based biosensor depending on whether the sensor uses living cells that express olfactory receptors or just the olfactory receptor protein itself as the sensing element. Various sensing techniques have been used to detect the binding of odorant molecules to olfactory receptor. Due to the recent development of efficient assay systems, the number of deorphanized receptors is increasing[15, 16].

2.1.1 Olfactory system

The mammalian olfactory system is a considerably sensitive organ that is capable of detecting and discriminating a wide range of different odorous chemicals at very low concentration. The olfactory system detects complex odorants by converting an odorant stimulus into an electrical signal, which is transmitted to the brain[5]. The perception of an odorant can be divided into two processes; odorant recognition, which occurs in the olfactory epithelium, and neural processing, which occurs in the olfactory bulb and higher cortical centers [1]. In vertebrate, the olfactory sensory neurons (OSNs) in the periphery are the primary sensing cells[17, 18]. A single dendrite reaches the surface of the tissue and ends in an knob-like swelling structure from which project some 20-30 very fine cilia[2].

When humans take a smell, odorants come into nose and reach the olfactory epithelium, which is covered by a thin film of watery mucus. Odorants are usually hydrophobic and are solubilized in the aqueous mucus with the help of odorant-binding proteins. After solubilization in the aqueous

mucus they reach the olfactory receptor on the cilia[19-21], where signal transduction takes place. The ciliary membrane contains olfactory receptor proteins, transducing components, ion channels, and certain enzymes[22]. The ciliary structure makes surface area increased , which allows for the effective capture of odorant molecules[23]. Each neuron has an unbranched axon that is projected towards the olfactory bulb at the front of the brain. The binding of odorants to olfactory receptors initiates an electrical signal, and this electrical signal travels along the axons into a region of the forebrain known as the olfactory bulb, which consists of glomeruli and neurons[24, 25]. The neurons transmit signals from the glomeruli to the olfactory cortex, where the signals are processed for odor discrimination[26-28].

2.1.2 Olfactory receptor and signal transduction

The first step in olfactory sensing is the binding of odorants to the olfactory receptors residing on the dendritic membrane of an olfactory sensory neuron[29, 30]. In vertebrates, a large family of G protein-coupled receptors (GPCRs) is involved in the recognition of odor signals. Buck and Axel showed that three percent of all human genes code for different odorant receptors. The gene family that encodes the olfactory receptors is estimated to consist of 1,000 genes in human, and about 70% of these genes are pseudogenes which do not encode a full-length polypeptide because of frameshifts, nonsense mutations, and deletions[31, 32]. Each olfactory neuron has a single type of olfactory receptor gene, and each type of receptor is expressed in thousands of neurons.

Since each receptor responds to several different odor molecules, humans can detect at least 10,000 distinct odorants. Olfactory receptors have seven hydrophobic transmembrane domains and several amino acid sequences are conserved in the olfactory receptor family. In addition, the expression of olfactory receptors is difficult in heterologous cell systems because they lack an N-terminal signal sequence. Furthermore, there are two signal pathways that are induced by olfactory receptor-odorant binding: the cAMP pathway and the inositol triphosphate (IP_3) pathway[33, 34].

When odorants bind to olfactory receptors, each olfactory receptor undergoes a conformational change and activates a G protein. The G protein is a heterotrimeric protein composed of three protein subunits: α, β and γ. When stimulated by odorant-receptor binding, the α subunit releases its bound guanosine diphosphate (GDP), which allows guanosine triphosphate (GTP) to bind. The binding of GTP to the α subunit causes a conformational change in the G protein, which in turn causes the dissociation of the α subunit from the βγ complex. The activated α subunit of the G protein then stimulates adenylyl cyclase (AC) and phospholipase C (PLC) to synthesize cAMP and IP_3 as a second signal transducer, respectively[27]. Odorants do not usually activate both the cAMP and IP_3 pathways, that is, the cAMP pathway and IP_3 cascade appear to operate as two alternative pathways[35]. However, it has been shown that odorants can trigger both pathways at high odorant concentrations.

Most vertebrate species use the cAMP signal pathway. The secondary signal transduction pathway for the cAMP response has been studied extensively, whereas the pathway for the IP_3 response is still unclear and

controversial.

The resulting transient rise in the cAMP concentration opens cyclic-nucleotide-gated (CNG) channels in the plasma membrane[36]. The inward current of Na^+ and Ca^{2+} through the CNG-channels causes an outward current of Cl^- through the Ca^{2+} gated Cl^- channels, thereby depolarizing the ciliary membrane. This depolarization then elicits the generator potential. The resulting electrical signal is transmitted along the axon and the action potential is then conducted to the brain via the olfactory bulb.

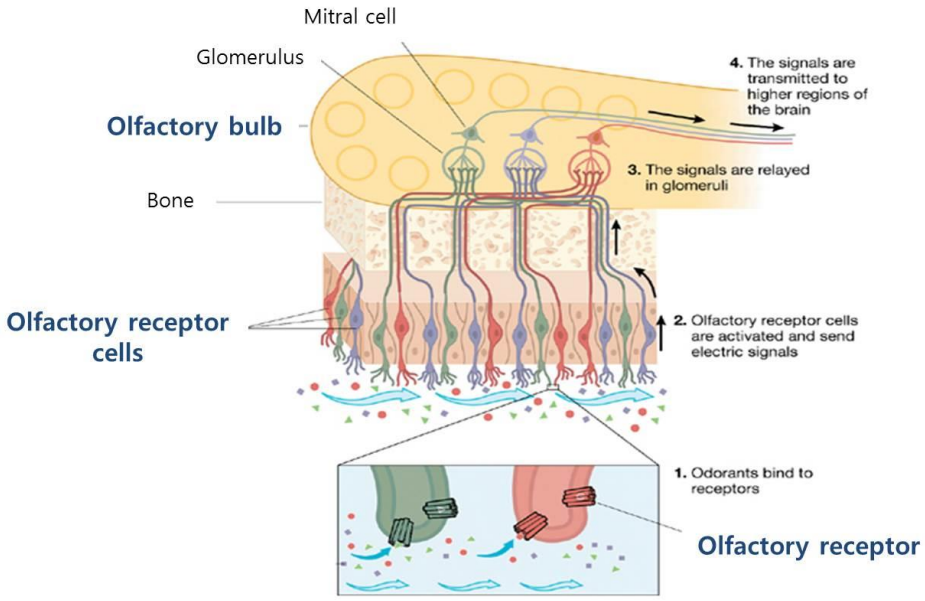

Figure 2.1 Human olfactory system. When odorant binds to the olfactory receptor, which is expressed in the olfactory epithelium, the electrical signal is generated and transmitted to the olfactory bulb along with the axons. Then the signal is transmitted to the higher region of the brain which controls thought and behavior (*Nature*, 2001, **413**, 211-218).

2.2 Odorant screening system

For many organisms, olfaction is a highly sensitive detecting system that can efficiently discriminate different odorous chemicals. This olfactory system has much more sensitivity and selectivity than the electronic nose, which use chemical sensing materials. Recently, many researchers world-wide have been trying to develop artificial sensing devices that are based on the olfactory system. A heterologous cell system, which uses live cells expressing olfactory receptors as the sensing element, can mimic a mammalian olfactory system; thus this method has the potential and capacity to be used as a biosensor and also provide biological information about mammalian olfaction. Various cell-based odorant detection methods, such as cAMP assay[37], Ca^{2+}imaging[38, 39], CRE reporter assay[40], and other screening systems, have recently been developed.

2.2.1 cAMP assay

The first step in signal transduction in the olfactory system is the activation of the G protein and release of the G_{α} subunit after odorant - olfactory receptor binding. The released G_{α} subunit then activates the adenylyl cyclase to synthesize cAMP. Various mammalian cell systems such as HEK-293, COS-7, CHO-K1, HeLa, and PC12h cells have been used for the expression of olfactory receptors and activation of endogenous $G_{\alpha s}$ to determine the level of cAMP, which is determined using an enzyme immune-assay. A dose-

dependent increase in cAMP after stimulation with a specific odorant has also been observed in olfactory receptor-expressing mammalian cells[41]. The cAMP assay system has also been used to show that the transmembrane proteins RTP1 and RTP2 promote functional expression of olfactory receptors in mammalian cells[42]. A luciferase reporter gene assay with a zif268 promoter was also used to amplify the signal derived from an increase in the level of cAMP upon odorant-stimulation with high sensitivity.

2.2.2 Calcium imaging

A Ca^{2+} imaging technique has been one of the most reliable and common methods to characterize the function of GPCRs including olfactory receptors [43]. Ca^{2+} play an important role in regulating the sensitivity of smell in the olfactory system[44, 45]. This approach has been used to greatly increase our understanding of Ca^{2+} signaling pathways and to show that CNG channels play a major role in Ca^{2+} influx. When odorants bind to olfactory receptors expressed in olfactory sensory neurons, the α subunit is released from the hertermeric G protein. The released α subunit then activates adenylyl cyclase to synthesize cAMP as a secondary messenger, which in turn opens the CNG cation channel. An influx of Ca^{2+}, which enters through this channel, results in an increase in the intracellular Ca^{2+} level[46]. In another pathway, IP_3 is synthesized as a secondary messenger[47, 48]. The synthesized IP_3 will then open ion channels in the plasma membrane and ER, which allows Ca^{2+} and Na^{+} to flow into cells. Ca^{2+} imaging methods can be used to detect the influx of Ca^{2+}

into cells. Changes in the intracellular concentration of Ca^{2+} ions can be measured using membrane-permeable Ca^{2+} fluorophores. The fluorescent emission of these Ca^{2+} fluorophores is sensitive to calcium concentrations such that their emissions intensities and wavelengths can be used to measure Ca^{2+} concentration changes inside cells. This strategy has been successfully used to detect odorants in cell-based assays. This method was used to detect a change in intracellular Ca^{+2} levels in HEK-293 cells co-expressing G_{α} and an olfactory receptor after stimulation with an odorant that was specific to the expressed olfactory receptor[41, 49, 50]. The first characterized human olfactory receptor OR17-40, which specifically binds to helional, was found using the Ca^{2+} imaging technique[51, 52]. The OR17-40 was cloned and functionally expressed in HEK-293 cells, and when a mixture containing a hundred of odorous chemicals (Henkel 100) was applied, a transient calcium signal was induced. Stably transfected cells displayed a stronger response to the odorant stimulus than transient transfected or mock transfected cells. Another example that highlighted the advantages of Ca^{2+} imaging was in a study that examined the effects of the agonist and antagonist on the human testicular olfactory receptor, hOR17-4[53]. As a result of the Ca^{2+} imaging technique, more human olfactory receptors have been characterized and the number of characterized olfactory receptors is increasing[54-56].

2.2.3 CRE reporter assay system

Odorants also can be detected by fluorescence or luminescence produced

by a reporter protein expressed upon odorant stimulation. In the cAMP response element binding protein (CREB)-related signal pathway, one of the various signal pathways of G-protein coupled receptors (GPCRs), including ORs, elevation of intracellular cAMP activates protein kinase A (PKA)[57]. Then, PKA moves into the nucleus and phosphorylates CREB, allowing it to bind to a CRE site and induce downstream gene transcription[58-61].

The most frequently used transcription products are green fluorescence protein (GFP) or luciferase. Salto *et al.* used CRE-luciferase to measure OR responses to odorants. When odorants stimulate ORs, expressed luciferase oxidizes luciferin and, in the process, luminescence is emitted[40, 62]. They also used various accessary proteins to enhance the expression of the luciferase upon odorant stimulation.

2.2.4 Bioluminescence resonance energy transfer (BRET) assay

Bioluminescence resonance energy transfer (BRET) assay is one of the methods of detecting odorant molecules using luminescence and fluorescence measurement[63, 64]. Mashukova *et al.* constructed a hOR2AG1-*Renilla* luciferase plasmid and β-arrestin2-GFP to detect the interaction between the OR and β-arrestin2. β-arrestin2 molecules were found to interact with ORs during ligand binding; in this experiment, when hOR2AG1-*R*luc bound to its specific odorant, amylbutyrate, the β-arrestin2-GFP interacted with hOR2AG1-*R*lus. A BRET signal was generated through the transfer of energy

from *R*luc, which released energy during oxidization of the substrate to an energy acceptor, GFP, resulting in the emission of light. In this experiment, BRET signal increased when the agonist amylbutyrate was applied to hOR2AG1. At another study, Dacres et al. detected the BRET signal generated by conformational change of OR upon odorant binding. They inserted GFP sequence in the third intracellular loop and Rluc at the C-terminus of ODR-10 and detected the BRET signal in femtomolar level by adding the diacetyl, which is specific to ODR-10[63]. The BRET assay, therefore, can be considered as a useful tool to monitor odorant-receptor interactions[64].

2.3 Bioelectronic nose

The bioelectronic nose constitutes a different sensor system compared to that of an electronic nose. Electronic noses, which use a chemical-sensing element, operate based on the detection of a mixture of odorants with a broad spectrum[13, 65]. Thus, these sensors have limitations as well as high cost when used as highly sensitive and selective sensors. In recent years, to supplement the shortcoming of electronic noses, many researchers have studied and developed artificial olfactory sensors based on biomaterials such as mammalian cells or proteins. Cell- or protein-based olfactory biosensors can be used as powerful and effective tools to discriminate a variety of odorant molecules with high sensitivity and selectivity. However, due to the complexity of the signaling process of the mammalian olfactory system,

wherein numerous biochemicals participate, there are many difficulties in developing a biosensor that mimic the olfactory system.

Olfactory biosensors are divided into two kinds of sensors depending on the sensing element used: cell and protein-based. The former utilizes live cells expressing olfactory receptor proteins[66-69], whereas the latter utilizes olfactory receptors themselves[70-72]. Cell-based olfactory biosensors, which use heterologous cell systems to express olfactory receptors, provide biological information about olfaction as well as potential as a sensor; these sensors are based on signal transduction in live cells. On the other hand, protein-based biosensors detect the direct binding of olfactory receptors to odorants. Olfactory biosensors consist of a primary transducer and a second transducer. The primary transducer is the biological recognition element of molecules such as cells and proteins. The second transducer is the biochip hardware platform for the detection of binding of odorants to the primary transducer. Various devices have been developed as a secondary transducer, and they are used in, quartz crystal microbalance (QCM), surface plasmon resonance (SPR), microelectrodes, nanotube-field effect transistor (FET), and others.

2.3.1 Quartz crystal microbalance

QCM has been used as a secondary transducer for odorant detection system[73, 74]. Since the QCM, as a piezoelectric crystal sensor, can detect the interaction between small molecules, many researchers used the QCM to

detect the odorant by coating the QCM surface with various sensing element such as polymer, lipid, enzyme, peptide and protein. QCM has several advantages such as simplicity, high sensitivity, and convenience. The principle of QCM is that, when a specific gas molecules bind to the coating material of QCM, the total mass of the surface increase and this mass change reduces the resonant frequency of the crystal[75]. The mass of concentration of the bound gas can be quantified using Sauerbrey equation as follow.

$$\Delta F = - F \Delta m / (A r t)$$

In this equation, ΔF is the change in resonant frequency (Hz), F is the initial crystal frequency (MHz), A is the total surface area (cm^2), r is the density of crystal (g/cm^3) and Δm is the mass adsorbed (g) on the surface. Due to the ability of QCM to quantitatively detect gas molecules, many researchers have tried to construct odor-sensing system using chemically modified QCM surface. For example, Wyszynski et al. used pegylated lipid and Koshets et al. used calixarene films as a coating material of the QCM surface to detect various odorous molecules such as alcohols, esters, acids, and aldehydes[65, 76, 77]. However, the chemically modified QCM showed low sensitivity and selectivity, so it was difficult to discriminate the structurally similar molecules.

The QCM sensor, functionalized with olfactory receptor is a useful odorant sensing system to detect and discriminate the various odorants with high sensitivity and selectivity. Several researches show that the QCM can be a good odorant sensing device by combining with olfactory receptor. Wu et al.

coated a QCM with olfactory receptors isolated from bullfrogs in order to construct an odorant sensor. Phosphotidylcholine, phosphotidylinosital and bovine serum were used as the coating material as the controls. In this study, only the QCM coated with bullfrog olfactory receptor showed a significant change in frequency upon odorant simulation. In another study, the *C. elegans* olfactory receptor ODR10 was heterologously expressed in *E. coli* and the purified protein was used as a sensing material of the QCM system. When the specific ligand diacetyl was injected in the range of 10^{-12}-10^{-5} mM, the frequency changed in dose-dependent manner and the response was highest to diacetyl among the various odorants which have similar functional structure[70]. The olfactory receptor which was expressed in mammalian cell was also used as a sensing material of QCM system. Ko and Park seeded the HEK-293 mammalian cell expressing the olfactory receptor I7 and incubated on the surface of the quartz crystal. When it is exposed to various odorants, the response was especially high for octanal, which is a known specific odorant of I7 and when it is exposed to various concentrations of octanal, the resonant frequency change increased in a dose-dependent manner[71]. In another studies, olfactory receptor-based synthetic polypeptide was deposited on the QCM to detect the low concentration of acetic acid. In this study, the QCM detect the acetic acid at 10 ppm[78]. These results clearly demonstrate that the piezoelectric system can be a useful odorant detection device with high selectivity and sensitivity. Moreover, because the system is based on the mass change, the quantitative analysis of odorant binding can be possible.

2.3.2 Surface plasmon resonance

The surface plasmon resonance (SPR) technique is an optical method that used a surface plasmon wave to monitor the change on the sensor surface[4]. Surface plasmon, which is an optical phenomenon, is the fluctuation in electron density in a solid or liquid by incident light. SPR occurs in free electron-like metals such as silver and gold. The electrons in a metal continuously move freely like a charged cloud. The resonance condition is established when light is focused onto the surface of the SPR followed by the energy is transferred from the light to the electrons in the surface. The critical angle, where the reflectance falls to zero, is called the resonance angle. The reflectance alters by any surface changes or binding events near the surface of SPR. Thus, the SPR system has been used as a biosensor to detect the interactions of various biomolecules in real time without labeling[79-81]. The use of SPR for biosensing was first demonstrated in 1983[82]. Since then, SPR has been widely used in biological applications such as ligand screening, cell biology, signal transduction, DNA-DNA, DNA-protein, protein-protein, and protein-lipid interactions[83-85] Recently, ligand screening or cellular signaling of GPCR using SPR system has also been reported[68, 83, 86]. This technique also has been used to detect the odorant-OR binding by Vidic *et al.*[12]. In this experiment, Rat ORI7 was co-expressed with $G_{\alpha olf}$ in a yeast expression system and nanosomes containing ORI7 were obtained by mechanical disruption. The nanosomes were immobilized on the surface of SPR and the desorption of the $G_{\alpha olf}$ subunit from the lipidic bilayer through the receptor

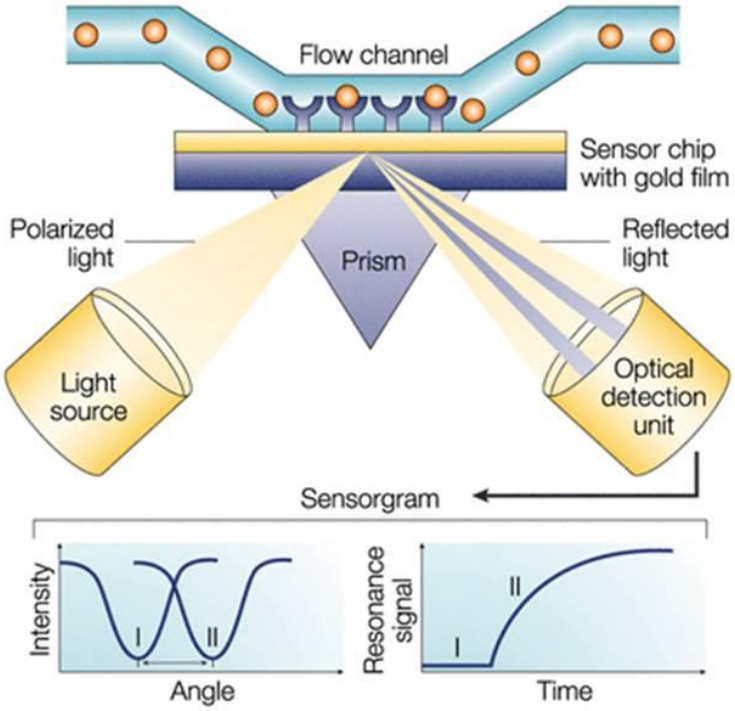

Figure 2.2 Principle of surface plasmon resonance (SPR). SPR system detects the change in refractive index in the surface layer of a sensor chip. The change in the sensor surface can be monitored by measuring the reflectance change or resonance angle shift in SPR system (*Nature Reviews Drug Discovery,* 2002, **1**, 515-528).

activation upon the odorant stimulation was monitored. Similarly, the nanosome containing human olfactory receptor hOR3A1 was obtained from yeast and used as a sensing material of SPR system[87]. Cell-based odorant detection using SPR system was also carried out in 2006 and 2009[88, 89]. The cells expressing ORI7 was cultured on the surface of SPR sensor chip and the reflectance change was measured upon odorant stimulation. When the various concentration of odorant was injected, the higher concentration of odorant induced a greater change in reflectance. And when the various odorants which have similar chemical structure was injected to the cells expressing ORI7, the cells responded to their specific ligand octanal in SPR system. In this study, it is showed that the SPR system can directly measure the odorant-induced cellular response. Besides, the SPR system was also used to study of a functional role of odorant binding protein[90-92].

2.3.3 Microelectrode

Microelectrode-based detection system has been used to measure the extracellular potential generated by ligand stimulation. This detection method, which is termed electrophysiological detection, has been conducted using patch-clamp, electrochemical impedance spectroscopy (EIS), and microelectrode array (MEA). Gomila *et al.* suggested that the characteristics of olfactory receptor might make it possible to construct an electronic olfactory nanobiosensor[93]. The idea was based on the concept with is that when the OR is bound to odorants, the conformational change occurs

and then might generate a change in the electrical property of the OR. Thus, the odorant binding can be detected by measuring the EIS. To demonstrate this, they manufactured nanovesicles containing ORI7 from the yeast membrane fraction by sonication and immobilized the nanovesicles on the gold surface of electrode via an antibody grafted SAMs or direct adsorption onto bare SAMs. Using this approach, a dose-dependent response of OR to specific ligand octanal was observed. Similarly, Hou *et al.* and Vidic *et al*. immobilized the ORI7 membrane fraction and hOR3A1 on the gold surface and conducted the measurement of change in electrochemical property, respectively[94, 95]. Microelectrode-based odorant detection system was also used in cell-based system. Lee *et al.* cultured the HEK293 cells expressing ORI7 and CNGgust channel on the four planer microelectrodes coated with poly- D-lysin[96]. The odorant binding to OR was detected by monitoring the generated field potential of the cells. The field potential response was the sum of the responses generated from the cells on each electrode. When the cells were stimulated with the various concentration of odorant, the dose-dependent response was recorded by the planer microelectrode. In other experiment, they provided an additional transient electrical stimulation after the odorant injection to enhance the cellular response or the cells[97]. For another example, the measurement of the extracellular potential in intact olfactory epithelium using microelectrode array was reported in 2010 by Liu *et al*. In this experiment, the olfactory epithelium was isolated form the rats and placed on the 36 separated electrode surface[66]. The cellular activities at many sites were recorded simultaneously by multi-channel recording system and the signals

recorded from multi-channels were analyzed by relevant signal processing method. Thus, the odorant detection on the microelectrode-based system was possible in both protein- and cell-based system.

2.3.4 Field effect transistor

The nanometer-scale sensor based on field-effect transistors (NT-FETs) is a new technique in the field of chemical sensing. Recently, the single-walled carbon nanotube (swCNT) and the conducting polymer nanotube (CPNT) have been incorporated into electrochemical sensors to detect the odorant with high sensitivity and selectivity. Kim *et al.* introduced a swCNT-FET combined with human olfactory receptor as an odorant sensing system[72]. hOR2AG1, which is specific to amylbutyrate, was expressed in *E. coli* and the partially purified hOR2AG1 was spread onto the swCNT-FET sensor. To detect the odorant binding to OR, the source-drain current was monitored along the addition of amybutyrate. When the various concentration of amylbutyrate was added, the source-drain current sharply decreased and gradually reached to saturation value. This indicates that the binding of odorant to OR induced the change in current. The detection limit was 1 pM, which is significantly lower concentration than the concentration detected using different transducers. The swCNT-sensor also showed the specific detection of odorant when the various odorants, which have similar chemical structure, were added to the sensor. In other experiments, nanovesicle containing OR was used as a sensing material in CNT- FET sensor system. Jin *et al.* obtained nanovesicles from mammalian

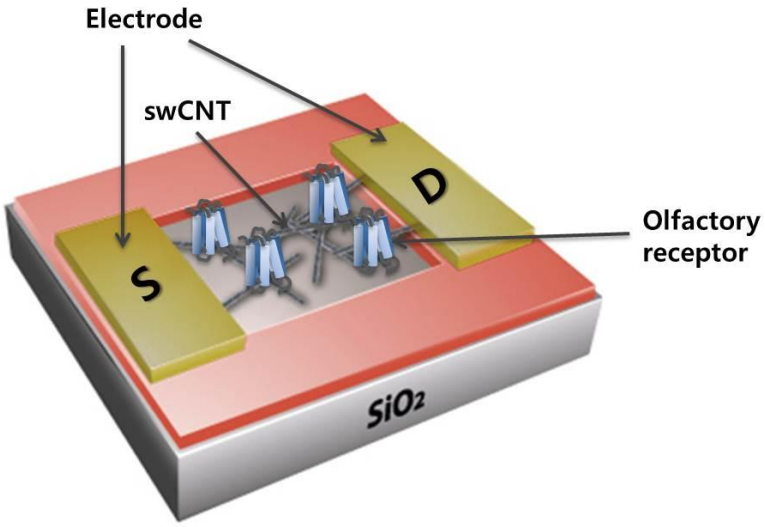

Figure 2.3 swCNT-FET sensor combined with human olfactory receptor. The source-drain current was monitored along the addition of odorant. When the odorant binds to OR, the current is changed.

cell expressing hOR2AG1 by the agitation in the presence of the cytochalasin B[98]. The nanovesicles containing hOR2AG1were immobilized on swCNT-FET and the activity of the nanovesicles upon ligand stimulation was monitored. They carried out the experiment using nanovesicle in PBS solution with or without calcium ions. While the activity of nanovesicle in PBS with calcium ions was detected, any response was not detected in PBS without calcium ions. Thus, the activity of the nanovesicles was generated from cellular signaling pathway, which the calcium ions enter into cells upon ligand stimulation. *Lim et al.* used the nanovesicle-based swCNT-FET sensor as a diagnosis tool to detect the molecules produced from lung cancer patient[99]. The peptide-based swCNT-FET for odorant detection using olfactory receptor-derived peptide was also reported[100]. Yoon *et al*. fabricated the FET sensor platform based on hOR2AG1-conjugate conducting polymer nanotubes[101]. hOR2AG1 was immobilized onto a CPNT, and the odorant-OR binding was detected by measuring change in current. Otherwise, the interaction of odorant and OR can affect the charge-carrier density of conjugated CPNT, and thus generated the source-drain current. The detection limit of this sensor was tens of femtomoles. In 2012, Lee *et al*. used CPNT-FET to detect odorant in gaseous phase[102]. Human olfactory receptor hOR3A1, which was expressed in *E. coli*, was immobilized onto the CPNT-FET and exposed to its specific ligand helional in gas phase to mimic the natural olfactory mechanism. They named this system the human-like nanobioelectronic nose (nbe-nose). The minimum detectable level of the nbe-nose was 0.02 ppt which is highly sensitive to other gas-phase sensor. These

results shows that the natotube based-FET system combined with olfactory receptor or nanovesicle containing OR can be used as a highly sensitive odorant detection sensor and can also be applied to various areas which need to detect or diagnosis the meaningful odorant molecules.

2.4 Visualization of smell

In order to discriminate among thousands of odors, we do not have any reliable sensing device, but still depend on our sensory system. However, the information obtained through the sensory system does not provide us with the objective information about the odors. Up to now, complex experimental steps, large-scale equipment, well-trained expert or electronic nose has partially played a role for the detection or analysis of odors. In addition, it is difficult to collect the data on the odorant response pattern to be used as an objective index [103]. However, if the odor is visualized, the visualized pattern can be used as code for smell.

Several cell-based odorant screening systems detect the odorant with the visualization techniques. Calcium imaging method, which is the most widely used odorant detection method[105], uses the fluorescent calcium indicator flou-4 or fura-2 to detect the calcium influx generated by the OR-odorant binding. And the BRET assay detects the odorant binding with bioluminescence generated by the intracellular signaling. Although these methods detect the odorant using visualizing techniques, they focus only on the odorant screening

but not on the visualization of odorant response and binding pattern. In addition these methods are limited to be used for the visualization of odorant response because the systems are the labor-intensive and time-consuming processes to apply to the various olfactory receptors simultaneously and largely dependent on the cellular condition.

The visualization of smell is the process to suggest the code for smell. Individual person can recognize the smell differently depending on the own experience; however, if the smell can be represented by objective data in the molecular level using visualization technique, the discrimination of smell can be systematically conducted and the index of smell can be used as a useful information in various applications.

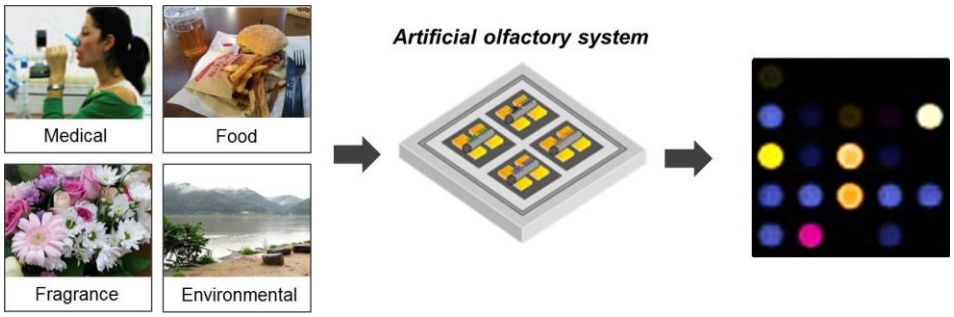

Figure 2.4 Visualization of smell. If various smell can be visualized, the visualized pattern can be used as a code for smell.

Chapter 3.

Materials and Methods

Chapter 3. Materials and Methods

3.1 Molecular cloning

3.1.1 Cloning of hOR genes

The human olfactory receptor genes were amplified from human genomic DNA using poly chain reaction (PCR) technique. For the expression of hOR in *E. coli*, hOR gene was cloned into the Gateway vector pDEST-15, which encodes the gene of glutatione S-transferase (GST) as a fusion partner at N-terminus. And for the expression of hOR in mammalian cell, hOR genes were cloned into the pcDNA3 vector. A Rho-tag was subcloned into the pcDNA3 using BamHI and EcoRI restriction enzyme sites. hOR genes were amplified by PCR using primers containing EcoRI and XhoI or EcoRV and XhoI sites. After digestion with the above restriction enzymes, the receptor genes were inserted into pcDNA3 digested with the same restriction enzymes. To enhance the expression of hOR in cell membrane, RTP1S was amplified from the RTP1L plasmid (Origene, Rockville, MD, USA) and cloned into pcDNA3. Human $G_{\alpha olf}$ gene was cloned into pcDNA3.1.

3.1.2 Construction of plasmid vector containing CRE reporter system

The pcDNA3-CRE reporter vector was generated by PCR-based subcloning of the destabilizing domain (DD)-CRE-ZsGreen gene from pCRE-DD-

ZsGreen1 (Clontech, Palo Alto, CA, USA). The original promoter of pcDNA3 was deleted and NheI site was created by mutagenesis and the (DD)-CRE-ZsGreen genes were inserted into pcDNA3 using Nhe I and XbaI sites. 2, 4, 12 CRE sites were inserted into pcDNA3 using NheI site.

3.1.3 Construction of ion channel-coupled hORs

Human potassium channel Kir6.2 was coupled to the four different human olfactory receptor hOR2AG1, hOR1A2, hOR3A1 and hOR1G1 to construct the ion channel-coupled ORs (hOR-Ks). Human olfactory receptor genes were amplified from human genomic DNA and inserted into EcoRI/XhoI sites or EcoRV/XhoI sites of pcDNA3. Rho-tag sequence was inserted at 5' end of the hOR gene for membrane expression of the hOR protein. Since Moreau et al. reported that the first 25 residues deleted-ion channel shows the optimal efficiency when coupled to GPCR[107], the hOR was also coupled to the first 25 residues deleted-ion channel. The human Kir6.20-25 gene from which the genes coding the first 25 amino acids were deleted was amplified from its original clone pCMV6-ENTRY/Kir6.2 (Origene, USA) using PCR with complementary primers containing Sal I and Xba I sites. The hOR-Ks were created by insertion of Kir6.20-25 gene at 3' end of the hOR genes cloned into Xho I and Xba I sites of pcDNA3. The hOR2AG1-(6G)-K was created by the addition of hexaglycines between the hOR2AG1 and the Kir6.20-25 genes.

3.2 Expression of hORs

3.2.1 Expression of hOR in *E. coli* system

The human olfactory receptor hOR3A1 gene was cloned into the Gateway vector pDEST-15, which encodes the gene of glutatione S-transferase (GST) as a fusion partner at N-terminus. The *E. coli* BL21 strain was transformed with pDEST-15/hOR3A1 and then cultured in lysogeny broth (LB) medium at 37˚C. When the optical density (O.D.) value reached 0.5, 0.5 mM of isopropyl β-D-thiogalactoside (IPTG) was added to induce the expression of hOR3A1 and the production of OR protein continued for 4 h.

3.2.2 Expression of hOR in mammalian cell system

3.2.2.1 Electrophoration

HEK-293 cells were maintained in Dulbecoco's modified Eagle's medium (DMEM) supplemented with 10% fetal bovine serum (FBS) and 1% penicillin/streptomycin. The cells were treated with trypsin and resuspended to a density of 1.5 x10^7 cells/mL with PBS buffer. 100 μL of the cell solution was mixed with 5 μg of pcDNA3 containing hOR or each hOR-K. Then the mixture was exposed to the electrical pulses using Neon Transfection System (Invitrogen, USA) at the operating condition of 1100 v, 10 ms, and 3 pulses.

And the transfected cells were seeded in the 96 well-plate and incubated in the DMEM/10% FBS without penicillin/streptomycin at 37 ℃. The cellular density was 8×10^4 cells/well and the volume of medium was 100 µl/well. The transfected cells were cultured for 48 h.

3.2.2.2 Lipofectamine

HEK-293 cells were trypsinized and resuspended to 4×10^6 cells/mL with DMEM. The cells were transfected with 5 µg of pcDNA3/hOR, 0.3 µg of pcDNA3.1/$G_{\alpha olf}$, 0.3 µg of pcDNA3/Ric8b and 0.3 µg of pcDNA3/RTP1S using lipofectamine2000. The transfected cells were seeded to poly-D-lysin-treated polycarbonate membrane and cultured for 48 h.

3.2.2.3 Reverse transfection

The aqueous gelatin solution was prepared as follows. Gelatin (1.2%, w/v) was dissolved in pure water by heating at 55℃ for 20 min. The solution was slowly cooled to room temperature and was filtered with a 0.45 µm cellular acetate membrane. A 4 µL aliquot of OptiMEM (Invitrogen, Carlsbad, CA, USA) containing 0.4 M sucrose, 2 µg plasmid DNA (pEGFP-N1 or pDsRed-N1), and 4 µL Lipofectamine 2000 (Invitrogen) were mixed to test the reverse transfection efficiency on the PEG microwell. After incubating the mixture at room temperature for 20 min, 2 µL of 1.2% gelatin solution was added and gently mixed to make a final gelatin concentration of 0.2%. To assay the signal generated from binding of the hOR and odorants, 2 µg pcDNA3/hOR

vector, 0.3 μg pcDNA3.1/$G_{\alpha olf}$, and 0.2 μg pcDNA3/RTP1S were mixed with transfection reagents and gelatin solution. The plasmid DNA/gelatin mixtures were spotted onto the PEG microwells using a MicroCaster™ 8-pin System (Whatman, Florham Park, NJ, USA). The spotted glass was dried in a vacuum desiccator for at least 12 h. HEK293-12CREs cells were seeded on the spotted PEG microwell glass and cultured for 48 h to express the hORs or fluorescence proteins.

3.2.3 Confirmation of the expression of hOR

3.2.3.1 Western blot analysis

The protein expression was confirmed after 48 h by immunocytochemistry and Western blot using anti-rho or anti-Kir6.2 antibody. For the immunocytochemistry, the cells were fixed with absolute ethanol at -20℃ for 15 min, and then the cells were incubated in Tris-buffered saline containing 0.1 % of Tween-20 (TBST) containing anti-rho antibody as a primary antibody (GenScript, USA, 1: 500 for 2 h) and anti-rabbit antibody conjugated with Alexa-594 as a secondary antibody (Invitrogen, USA, 1:1000 for 1 h). For the Western blot analysis, the cells expressing the ion channel-coupled OR were trypsinized and sonicated (2 s on/off, 1 min) followed by the centrifugation at 12,000×g for 30 min to collect the membrane fraction. The hOR-K proteins, which were expressed in the membrane fraction, were detected using anti-Kir6.2 antibody (Santa Cruz, USA, 1:2000 dilution with 1%

skim milk in TBST), as a primary antibody, and HRP-conjugated anti-goat antibody (Amersham, USA, 1:2000 dilution with 5% skim milk in TBST), as a secondary antibody.

3.2.3.2 Immunocytochemistry

The cells were fixed in -20℃ ethanol for 15 min for immunocytochemistry. After fixation, the cells were washed with phosphate buffered saline (PBS) and incubated in PBS containing primary rabbit anti-rho antibody at 1: 500 for 2 h. After washing with PBS, the cells were incubated with the secondary anti-rabbit antibody conjugated with Alexa-594 at 1:1000 for 1 h and were imaged by fluorescence microscopy.

3.3 Reconstitution of hOR

3.3.1 Purification of hOR from *E. coli*

The cells were collected by centrifugation at 12,000xg for 5 min and resuspended in phosphate buffered saline (PBS) buffer containing 1% of Triton X-100. After the cells were lysed by sonication for 5 min (5 s on/off), the insoluble fraction was collected by centrifugation at 12,000xg for 30 min. The treatment of Triton X-100 removed the impurities except hOR3A1, and hOR3A1 was extracted by incubation with PBS buffer containing 0.5% sarcosyl for 1 hour. The fraction containing hOR3A1 was collected by centrifugation at 12,000xg for 30 min. For further study, the buffer was

replaced with HEPES-buffered saline (HBS) containing 8 mM of Chapso.

3.3.2 Reconstitution of hOR using liposome

As a next step, 8 mg of egg phosphatidylcholine (eggPC) was dissolved in chloroform in a glass flask and the solvent was evaporated using N_2 gas stream followed by drying at a vacuum chamber for 20 min resulting in the formation of eggPC film. The eggPC film on the glass was dissolved in HBS buffer containing 8 mM of Chapso until final concentration of eggPC reached 2 mM. The lipid/detergent micelles were formed using a freeze and thaw method five times. The partially purified hOR3A1 proteins were concentrated using membrane filtration and resuspended in HBS containing 8 mM of Chapso. The concentration of Chapso was determined by measurement of O.D. at 450 nm as the Chapso was added to eggPC liposome by increasing its concentration. The hOR3A1 proteins were then added to eggPC/Chapso mixed micelles and the mixture was gently shaken for 1 hour. To form the liposome containing hOR3A1, SM2 bio-bead was added to the solution and incubated to remove the Chapso. The incubation time of SM2 bio-bead was also determined by measurement of O.D. at 450 nm.

3.3.3 Confirmation of reconstituted hOR

To confirm the correct insertion of hOR3A1 into the liposome, we

conjugated the hOR3A1 with Cy2, which emits green fluorescence, using Amersham FluoroLink^{TM}-Ab Cy2 labeling kit. Liposomes containing Cy2-conjugated hOR3A1 were immobilized on the poly D-lysine-treated glass substrate for 2 hr. After washing with HBS buffer solution several times, liposomes containing hOR3A1 were imaged by fluorescence microscopy. Cy2-conjugated hOR3A1 proteins were also confirmed by Western blotting analysis using anti-GST antibody (Santa Cruz, USA) as a primary antibody that was diluted by 1:2000 with 1% skim milk in PBS plus Tween 20 (PBST), and using HRP-conjugated anti-mouse antibody (Amersham, USA) as a secondary antibody that was diluted by 1:2000 with 5% skim milk in PBST.

3.3.4 Size control of liposome containing hOR3A1

The size of liposome was analyzed using ELS 8000 electrophoretic light scattering spectrophotometer (OTSUKA Electronics Co. Ltd., Japan). To control the size of liposome proper to SPR analysis, the suspension of liposomes was sonicated for 10 min (Branson Ultrasonics, USA) followed by the filtration using mini-extruder device (Avanti Polar Lipid Inc., USA).

3.4 PEG microwell-based odorant screening system

3.4.1 PDMS stamp fabrication

The master mold for the PDMS stamp was fabricated using standard soft

lithography. A photoresistor (SU-8 2075, Microchem, Newton, MA, USA) was spin-coated onto a silicon wafer (500 rpm, 5 sec; 2000 rpm, 30 sec), baked (65℃, 5 min; 95℃, 20 min), and was then exposed to UV light using a mask aligner (MA6, Suss MicroTec AG, Garching, Germany). After post-baking (65℃, 1 min; 95℃, 10 min), the stamp patterns were formed through a development process (10 min) using SU-8 developer (Microchem). The PDMS prepolymer (Sylgard 184, Dow-Corning, Corning, NY, USA) was mixed with its curing agent in a 10:1 ratio. After removing the bubbles by degassing, the mixture was poured onto the patterned silicon wafer and baked at 80℃ for 2 h. The cured PDMS was peeled off the master mold and used as a stamp.

3.4.2 PEG microwell fabrication

PEG microwells were fabricated using micromolding on UV-photocrosslinkable polyethylene glycol diacrylate (PEGDA, MW700) (Sigma-Aldrich Co., St. Louis, MO, USA) solution containing 0.5% (w/w) of the photoinitiator 2-hydroxy-2-methyl propiophenone. Glass substrates were treated with 3-trimethoxysilyl propylmethacrylate (TMSPMA) (Sigma-Aldrich) for 5 min and baked at 70℃ for 2 h. The PDMS stamp was placed on glass with 30% PEGDA solution, and the PEGDA solution was photocrosslinked upon exposure to 365 nm wavelength UV at an intensity of 10 mW/cm for 10 min. The PDMS stamp was peeled off after polymerization of the PEGDA solution, and the polymerized microwell was washed using

distilled water and dried with air. The diameter of the PEG microwell was 500 μm and the depth was 100 μm. The fabricated microwell on the glass substrate allowed cells to adhere to the bottom of each well.

3.5 Fabrication of microfluidic system for odorant detection in gas phase

3.5.1 Design and assembly of a microfluidic system for odorant detection in the gas phase

The device, which is used to monitor the response of cells expressing OR to gaseous odorant molecules, consists of two layers of PDMS, where the PDMS are sealed between the poly(methyl methacrylate) (PMMA) bottom and polycarbonate top frames (Ideatech, Hwaseoung, Korea). The top PDMS layer has a fluidic channel (4 mm wide, 24 mm long, and 1 mm deep). The bottom PDMS layer has a hole with a 5 mm diameter. The top PDMS layer is underneath the top PC frame. The bottom PDMS layer is on the bottom PMMA frame (Figure 1A and B). The top PC frame has two inlet/outlet holes (each with a 5 mm diameter), and the small holes of the top PDMS layer were punched (Technical Innovations Inc., TX, USA) to inject gaseous odorants into it. Tygon tubing (Fisher Scientific, PA, USA) was connected via a small steel tubing (New England Small Tube Corporation, NH, USA), which was inserted into the punched inlets and outlets of the PDMS through the inlet/outlet holes of the top PC frame (Fig. 3A and B). The cells were cultured

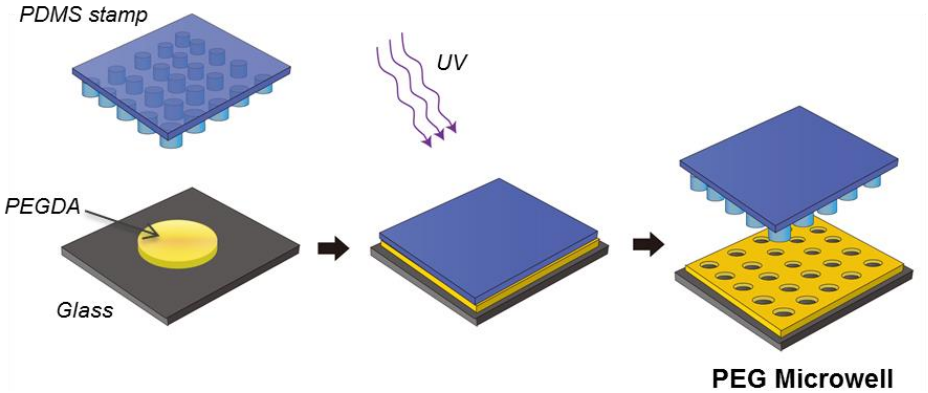

Figure 3.1 Scheme of the fabrication of PEG microwell. The PEGDA solution was dropped onto the TMSPMA-treated glass and was pressed with PDMS stamp. After UV exposure, the stamp was peeled off from the glass, then the PEG microwell was formed.

on the PC membrane. The membrane was flipped upside down and placed on the bottom PDMS layer after the layer's hole was filled with the cell culture medium. The device was assembled by sandwiching a membrane between the top PDMS layer with the PC top frames and the bottom PDMS layers with the bottom PMMA frame (Fig. 3D). The gaseous odorant molecules were collected using a 50 mL syringe from the bottle, where the odorant molecules were fully evaporated, and injected into the device using a syringe pump at a flow rate of 0.8 mL/s

3.5.2 Cell adhesion on the polycarbonate membrane

The polycarbonate (PC) membrane having 2 μm pore was treated with 0.05 % of poly-D-lysine for 2 h. Then, the PC membrane was washed with DW for three times. The HEK-293 cells were cultured in DMEM containing 10 % FBS and 1% penicillin/ steroptomycin. The cells were harvested and transfected with the vector containing hOR genes using lipofectamine 2000. The transfected cells were seed on the poly D-lysine treated PC membrane in the concentration of 4 x 10^6 cells/mL. The cells were cultured for 48 h for the expression of hOR.

3.5.3 Preparation of gaseous odorant

The odorants (bourgeonal, β-citronellol, and geraniol) were dissolved in dimethyl sulfoxide (DMSO) and diluted with distilled water to 1 mM. To

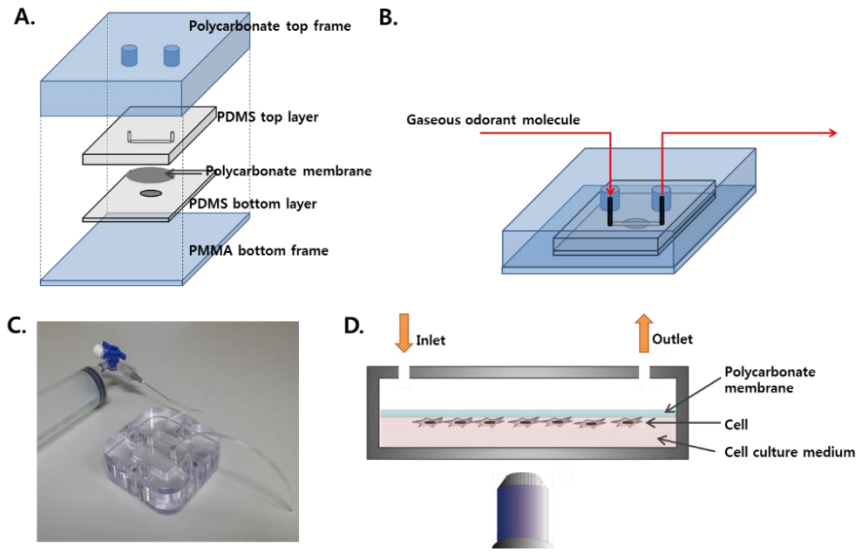

Figure 3.2 Schematic diagram of the microfluidic system for odorant detection in the gas phase. (A) Schematic diagram that shows how the device is assembled. The device is assembled by sandwiching a membrane between the top PDMS layer with the PC top frames and the bottom PDMS layers with the PMMA bottom frame. The sealing is performed with screws between the edges of the frame. (B) Schematic diagram of the assembled microfluidic device and the gaseous odorant molecule injection process. (C) Image of the assembled microfluidic system for gaseous odorant detection. (D) Schematic diagram of the side view of the microfluidic system for gaseous odorant detection. The membrane was flipped upside-down and placed on the bottom PDMS layer after the hole of the bottom PDMS layer was filled with the cell culture medium.

produce the gas samples, the odorant solutions were placed in 117 mL bottles sealed with a septum cap, and fully evaporated at room temperature. To produce 200, 100, 50 and 20 ppm of gas samples, 10, 5, 2.5, and 1 μL of the odorant solution (1 mM) were evaporated in the bottle.

3.6 Detection of odorant response

3.6.1 SPR analysis

For the SPR analysis, SPRi (K-MAC, Korea) and a sensor chip (18 mm x18 mm) with 50 nm thick of gold film were used. The gold surface used for the SPR measurements was treated with 0.1 mg/mL of poly D-lysine for an hour in 25˚C for the adsorption of liposome with ionic interaction and washed with desterilized water several times to remove free poly D-lysine. The sensor chip and prism (n_D = 1.515, BK 7) were contacted using a refractive index matching fluid (n_D = 1.515-1. 517, Merck). The SPR sensor chip was mounted in a liquid cell and exposed to the HBS buffer at 20 μl/min of flow rate. The reflectance shift was measured with a photodiode detector. Adsorption was initiated by replacing the buffer with buffer including liposomes containing hOR3A1. After adsorption of the liposomes, the buffer was changed to HBS buffer containing 1% DMSO in order to create the same buffer condition since the odorant solution contains 1% DMSO to efficiently solubilize the hydrophobic odorants. When the base line stabilized, the odorants solution was injected for 400 seconds at 7.5 μl/min and washed with buffer solution.

The negative control was the reflectance change on liposome not containing hOR3A1. The change of reflectance was detected every second and the temperature was kept at 25˚C during the experiment.

3.6.2 CRE reporter assay

HEK-293 cells were maintained in Dulbecoco's modified Eagle's medium supplemented with 10% fetal bovine serum and transfected with pcDNA3-CRE. Stable cell lines containing the reporter gene system (HEK293-12CRE cells) were selected using the antibiotic G418. The function of the selected HEK293-12CREs cells was tested with 10 μM forskolin, 1 μM Shield-1 and 0, 100, or 200 μM 3-isobutyl-1-methylzanthine (IBMX). Shield-1 plays a role to cover the DD, which is fused to the reporter gene and blocks basal expression of the reporter gene. Thus, Shield-1 was added with forskolin to induce expression of the reporter gene. After a 24 h incubation, the green fluorescence of reporter protein ZsGreen was detected by fluorescence microscopy. Cells expressing four different kinds of hORs (hOR3A1, hOR1A1, hOR1D2, and hOR1G1) via the reverse transfection method on PEG microwell were stimulated by their specific ligand with 100 μM IBMX and 1 μM Shield-1 to detect the odorant response. ZsGreen expression upon ligand stimulation was observed after a 24 h incubation. Cells expressing hORs treated only with IBMX and 1 μM Shield-1 were used as a negative control.

3.6.3 Membrane potential assay

To detect the change of membrane potential generated by positively charged- ion influx upon ligand stimulation, we used FLIPR Membrane Potential Assay Kit (Molecular Devices, USA). There are two assay kits containing red or blue membrane potential dyes. Two membrane potential dyes were tested and the red dye showed higher and more stable fluorescence change upon ligand stimulation than blue dye. Therefore we chose the assay kit containing red dye for the odorant response detection of hOR-K. After the cells were transfected with pcDNA3/hOR-K in 96 well-plate and incubated for 48 h, the 100 μL of membrane potential dye was added to each well. Then the mixture was incubated at 37 ℃ for 20 min. The odorants were prepared at a concentration of 1 M in DMSO and serially diluted in distilized water to a concentration from 2 nM to 200 μM. The 50 μL of each odorant was added to each well and the membrane potential change upon odorant stimulation was detected by spectrofluorometer (Tecan, Switzerland) at 535 nm for excitation and 590 nm for emission. The detection time interval was 5 s and the total detection time was 100 s. The membrane potential change was also detected by image scanning method using Typhoon 9410 (GE healthcare, USA) at 555/30 nm for excitation and 610/30 nm for emission. The scanning was conducted at the 200 μm resolution and the normal sensitivity mode.

3.6.4 Calcium imaging

Fluo-4, a calcium ion-sensitive fluorescent dye, was used for calcium imaging upon odorant stimulation. HEK-293 cells expressing hOR were incubated with the medium containing 5 μM of Flou-4/AM and 1 mM of probenecid at 37 ℃ for 30 min. Then the cells were washed with indicator-free medium and incubated for a further 30 min. The fluorescence generated by the odorant stimulation was detected using fluorescence microscopy at 488 nm for excitation and 535 nm for emission.

3.6.5 Image analysis

The fluorescence intensity of the image was calculated using ImageJ software. After the background correction, the fluorescence intensity was measured and plotted as a bar or line graph. To visualize the odorant response of hOR-Ks, the fluorescence images before and after the odorant stimulation were acquired using fluorescence image scanner and the background correction was carried out. The fluorescence images were normalized by subtracting the image before the ligand stimulation from the image after the ligand stimulation followed by median filter process and threshold adjustment. The pseudo color was assigned to the image through lookup tables in plug-in menu and the brightness/contrast range was adjusted.

3.7 Reagent

Chapso and eggPC for making lipid/detergent mixed micelle were purchased from Sigma-Aldrich. HBS buffer was made using 10 mM HEPES (pH 7.4) and 150 mM NaCl. SM2 Bio-beads was purchased from Bio-Rad Laboratories, Inc. All odorants [helional, safrole, piperonal, hydrocinnamaldehyde, 3-(3, 4 methylene diozyphenyl) propionic acid] were bought from Sigma-Aldrich. The 10^{-7} to 10^{-3} M of helional was prepared in HBS containing 1% DMSO. For the specificity test, all odorants were prepared in 10^{-4} M in the same buffer.

All odorant chemicals in this experiment (helional, β-citronellol, geraniol, and bourgeonal) were purchased from Sigma-Aldrich. Odorants were dissolved in DMSO at a concentration of 1 M as a stock solution and diluted serially with PBS to a concentration of 500 μM.

Chapter 4.

SPR-based odorant detection using liposome containing olfactory receptor

Chapter 4. SPR-based odorant detection using liposome containing olfactory receptor

4.1 Introduction

The binding of odorant to human olfactory receptor (hOR) is the first step of the odor-sensing mechanism in human olfactory system. It is well known that humans recognize and discriminate smell through a signaling cascade initiated by the binding of many different kinds of odorant molecules to approximately 390 different types of hORs but most ORs remain orphans. Hence, the identification of odorant molecules that bind to orphan hORs and the characterization of hORs is required to discover the function of orphan hORs[42]. For this purpose, various heterologous expression systems have been developed but the low expression efficiency of hORs has been an obstacle[108-112]. Moreover, the cell-based odorant detection system was easily influenced by environmental conditions. In case of other G protein-coupled receptors (GPCRs), the reconstitution of proteins using liposome or detergent was carried out to use the proteins as sensing materials in biosensor system in several researches[113, 114]. In this study, we expressed human olfactory receptor hOR3A1 in an *E. coli* expression system for high expression efficiency and stable odorant detection. The hOR3A1, which is mainly produced as an inclusion body in *E. coli*[115], was partially purified and reconstituted using lipid/detergent mixed micelles for stabilizing the structure of hOR3A1, which is a transmembrane protein. The reconstituted hOR3A1 was immobilized on

the gold surface of surface plasmon resonance (SPR), and the function of the odorant detection was analyzed. The results demonstrate that the reconstituted hOR3A1 can detect the specific odorant, helional, in a dose-dependent manner and can also discriminate it from odorants of a similar structure. Such a reconstituted olfactory receptor produced by *E. coli* expression system, can be useful as an efficient sensing material for the protein-based odorant detection system using various detection devices as well as using SPR.

4.2 Optimization to form the liposome containing hOR3A1

The olfactory receptor, which belongs to seven-transmembrane protein, is mainly produced as an inclusion body in *E. coli.* Therefore the reconstitution process to make it functional is the essential step for the study of ORs' function. In this research, hOR3A1 was expressed in *E. coli* (on average, 2-3 mg/L) and lipid/detergent mixed micelle was used to reconstitute the partially purified hOR3A1, which is known to specifically bind to a helional. We used Chapso for the preparation of detergent/lipid mixed micelle because Chapso is well known as a detergent more suitable to solubilize the GPCR[113, 116]. First, the critical micellar concentration was determined for the formation of lipid/detergent mixed micelle. Chapso was added into eggPC liposome increasing its concentration up to 14 mM and O.D. value was measured at every 2 mM interval at 450 nm wavelength. As shown in Fig. 4.

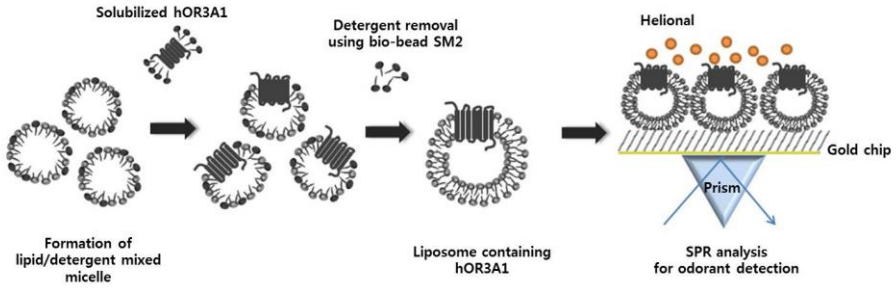

Figure 4.1 Schematic diagram of reconstitution of hOR3A1 and SPR analysis. The partially purified hOR3A1 was reconstituted using lipid/detergent mixed micelle and immobilized on the gold surface of SPR to detect the odorant binding.

2A, the liposomes were completely solubilized when the concentration of Chapso reached over 8 mM. Then Chapso was removed by adding SM2 bio-bead to the mixture containing 2 mM of eggPC and 8 mM of Chapso to reform the liposome. The O.D. of liposome was measured at 450 nm, and the results demonstrated that the detergent was completely removed during 2 hr incubation with SM2 bio-bead (Fig. 4. 2B). Thus, we used 8 mM of Chapso to form the detergent/lipid mixed micelle and finally this micelle was mixed with hOR3A1 solubilized in HBS buffer containing 8 mM of Chapso resulting in the formation of liposome containing hOR3A1.

4.3 Confirmation and size control of the liposome containing hOR3A1

To confirm that the hOR3A1 was inserted to eggPC/Chapso mixed micelle, we conjugated the hOR3A1 with Cy2, which emits the green fluorescence, prior to the formation of liposome. The liposomes containing Cy2-conjugated hOR3A1 were fixed on the poly D-lysin-treated glass substrate and imaged with fluorescence microscopy as shown in Fig. 4. 3A. The reconstitution of hOR3A1 in liposome was also confirmed by Western blotting analysis using anti-GST antibody (Fig. 4.3B). After the sonication for 10 min, the average diameter of the liposome containing hOR3A1 was 200~300 nm according to ELS analysis. We controlled the size of the liposome to 40~50 nm by extrusion, since the evanescent field on the SPR surface is formed efficiently

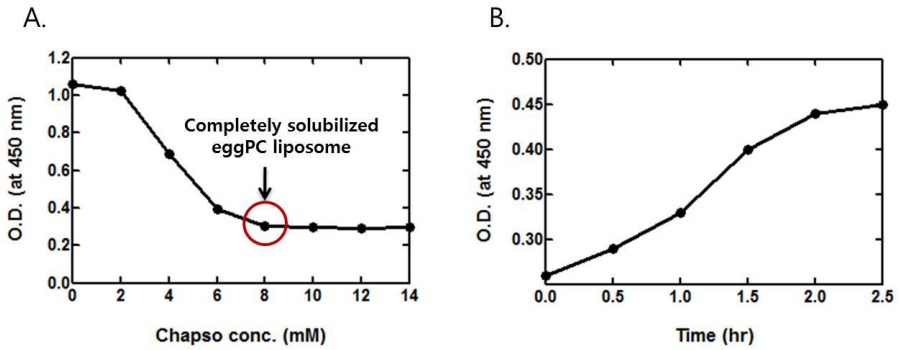

Figure 4.2 Determination of critical micellar concentration and the liposome formation by removing Chapso using bio-bead. (A) The 2 mM of eggPC liposome was completely solubilized when Chapso reached over 8 mM. (B) Chapso was removed by 2 hr incubation with SM2 bio-bead.

in ~200 nm (Fig. 4.3C). The size was the minimum size which we can control. Since it was unclear whether the hOR3A1 has functional structure and orientation in the liposome in this step, the functional assay of reconstituted hOR3A1 was carried out through SPR analysis.

4.4 Adsorption of the liposome containing hOR3A1 onto the surface of SPR

To analyze the function of reconstituted hOR3A1 using SPR, the liposome containing hOR3A1 was immobilized on SPR sensor chip. Various materials have been used to capture the protein on the gold surface such as antibody, peptide, and metal ions[80, 117, 118]. In this study, poly D-lysine was used to capture the liposome by administering positive charges on the gold surface of SPR sensor chip. The liposome was loaded on the poly D-lysine-coated SPR sensor chip at several flow rates (7.5, 20, 125 μl/min) to optimize the flow rate for efficient liposome adsorption. Since the negative charges of liposome interacted with the positive charges of the poly D-lysine-coated chip, the liposome containing hOR3A1 was able to be stably immobilized on the gold surface resulting in a gradual increase in thickness of the surface layer. The period for the saturated adsorption decreased with the injection flow rate; however, the final reflectance change was the same regardless of the change in flow rate. This indicates that the flow rate affects only the adsorption time, but not the amount of final liposomes that were adsorbed. We chose 20 μl/min

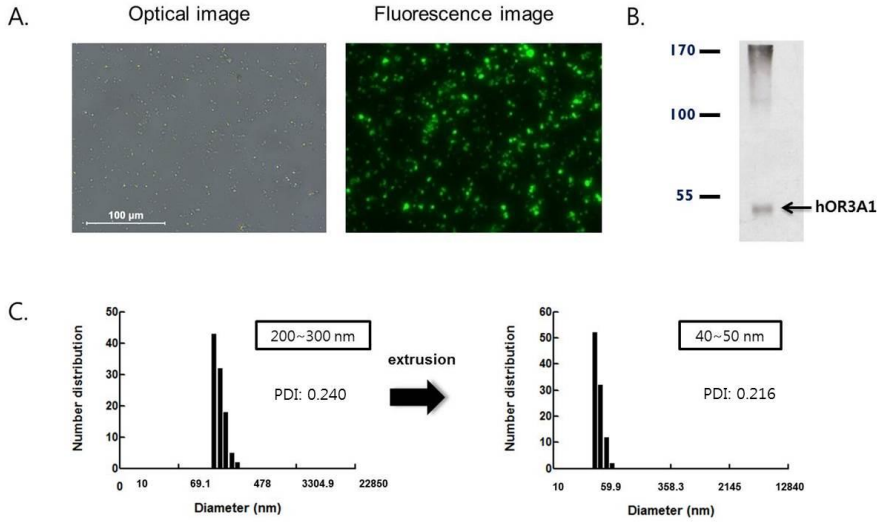

Figure 4.3 Confirmation of the presence of hOR3A1 in liposome. (A) Optical and fluorescence images of the liposome containing Cy2-conjugated hOR3A1 (B) Western blot image of hOR3A1 using anti-GST antibody (C) ELS result of liposome containing hOR3A1 after sonication and extrusion

of flow rate to detect the reflectance change upon liposome adsorption in subsequent experiments. As shown in Fig. 4.4, as the liposomes were adsorbed on the gold surface, the reflectance of SPR increased and reached saturation. The final reflectance change was about 7.5%.

4.5 Odorant binding activity test of the reconstituted hOR3A1 immobilized on the SPR gold surface

After the adsorption of liposome containing hOR3A1 on the SPR gold surface, the buffer was replaced with the HBS containing 1% DMSO. The baseline was newly established because all the odorants used in this study were dissolved in HBS buffer containing 1% DMSO. The activity of the immobilized liposome containing hOR3A1 was tested with 100 μL of helional at 7.5 μl/min of flow rate. Then, we injected the same solution to the hOR3A1-free liposome not containing hOR3A1 immobilized on the gold surface as a control. The reflectance was changed by 1% when the hOR3A1 was stimulated with 100 μM of helional for 500 sec, while the reflectance change of a control was only 0.2% (Fig. 4.5A). This result shows that the reconstituted hOR3A1 has a functional structure in liposome and binds to its specific ligand. The base line of liposome with hOR3A1 did not come back to the initial level even after the washing step. This is considered to be due to the high concentration of helional. It is considered that a buffer flow rate of 7.5 μl/min is not sufficient to completely wash the helional. In the experiment,

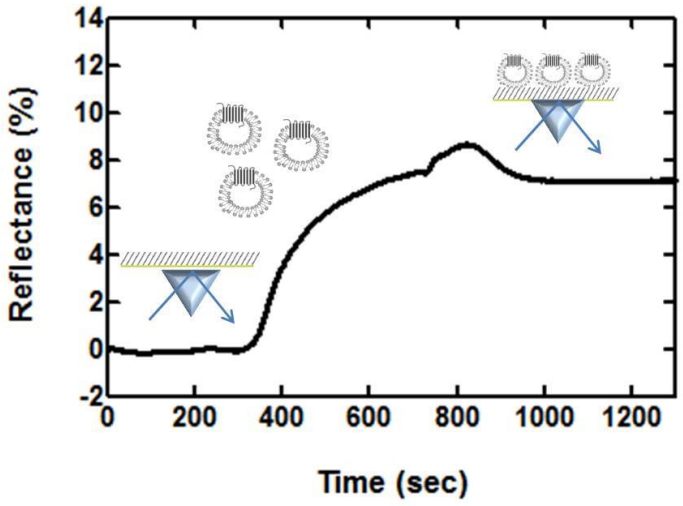

Figure 4.4 Adsorption of the liposome containing hOR3A1 on the poly D-lysine-coated SPR gold surface. The liposome was injected at 20 µl/min of flow rate and the final reflectance change after adsorption was 7.5 %.

with lower concentration of helional, the signal returned to the initial level. The slight change of reflectance in the control is considered as the non-specific binding signal by the adsorption of hydrophobic odorant molecules to the lipid component of liposome. But any reflectance change was not observed when 10^{-5} M or lower concentrations of helional were applied to the liposome without hOR3A1. To identify the dose-dependent response ofreconstituted hOR3A1, various concentrations of helional (10^{-7} to 10^{-3} M) were injected to the reconstituted hOR3A1 immobilized on the gold surface of SPR (Fig. 4. 5B) and the result shows that the reflectance change increased in proportion to the concentration of helional. The dose-dependent response curve has a sigmoidal shape in general. [42, 62, 101]. In this system, because of the solubility of helional, the SPR analysis was conducted below 10^{-3} M of helional. Thus the Fig. 4.5B shows the first half of the sigmoidal curve. According to the previous study, the dose-dependent response profiles have been reported in the range of 10^{-5} to 10^{-1} M in cell-based SPR analysis system [88]. Also, Vidic *et al*. reported that nanosome containing hOR3A1, which was generated from yeast expression system, responded to 5 μM of helional in SPR system [12]. In this study, the reconstituted hOR3A1 responded to 10^{-3} to 10^{-7} M of helional. This higher sensitivity was achieved because large quantity of hORs produced in *E. coli* system was reconstituted in liposome.

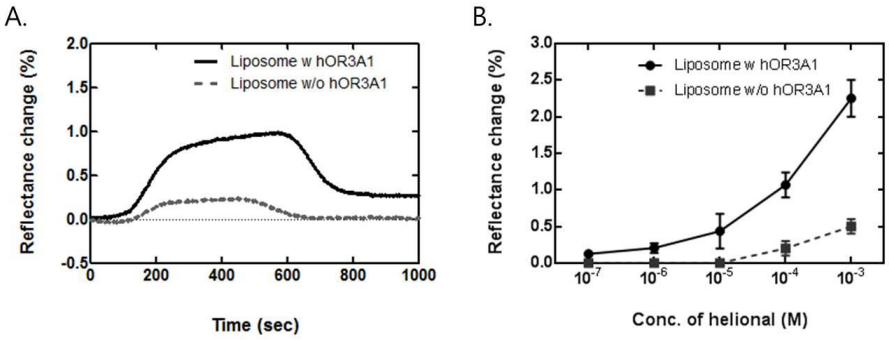

Figure 4.5 Detection of helional binding to hOR3A1 by SPR. (A) The reflectance was changed by 1 % when the liposome containing hOR3A1 was stimulated with 100 μM of helional, while the reflectance was changed only 0.2% in the case of the negative control. (B) Dose-dependent response of hOR3A1 to helional (n=3).

4.6 Selectivity of the reconstituted hOR3A1

The human olfactory receptor has the ability to selectively discriminate different structures of odorants. In this study, various odorants with similar chemical structure to helional [safrole, piperonal, hydrocinnam aldehyde, 3-(3, 4-methylene diozyphenyl) propionic acid] were tested for their selectivity of liposome containing hOR3A1. Each odorant was injected with the concentration of 10^{-4} M at 7.5 μl/min of flow rate. As a result, the highest reflectance change was observed upon the stimulation by helional, a specific ligand for the hOR3A1, while negligible changes of reflectance were detected by the stimulation with other odorants (Fig. 4.6). This result demonstrates that the functional analysis of reconstituted ORs using SPR technique was capable of effectively recognizing and detecting their specific target odorant.

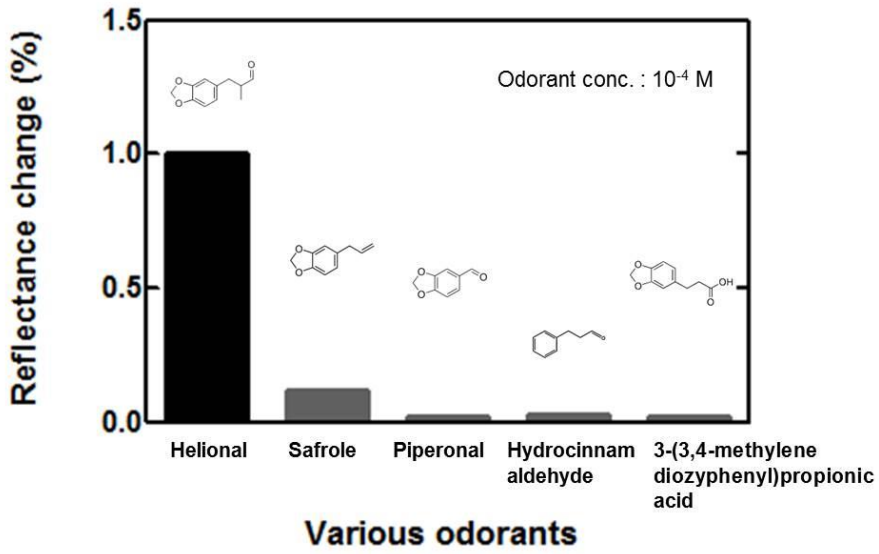

Figure 4.6 Odorant specificity of liposome containing hOR3A1. The highest reflectance change was generated from the stimulation with helional, while the slight change of reflectance was detected from treating other odorants with a similar structure to a helional.

4.7 Conclusions

Expression of olfactory receptors in the *E. coli* system has been regarded as a difficult job. Even if they are expressed, they are formed in an inclusion body. Therefore, various attempts have been made to develop alternative systems such as mammalian and yeast cell systems. However, these cell systems still have the disadvantage of low expression efficiency of hORs on the cell membrane. Together with these systems, the *E. coli* system has been investigated to overcome this drawback. It is important to make a functional structure and to provide a proper condition for hORs so that they can be used for the delicate biological study. In this study, hOR3A1, which was expressed in the *E. coli* system, was reconstituted using lipid/detergent mixed micelle and its function was analyzed by SPR. The reconstituted hOR3A1, which was immobilized on the SPR gold surface, showed the dose-dependent response to specific ligand and also showed the selectivity to discriminate its ligand odorant from other odorants. These results show that the large amount of hORs, which is expressed in *E. coli*, can be used as an efficient odorant sensing material by reconstitution for other odorant detection systems such as carbon nanotube, conducting polymer nanotube and graphene as well as the SPR-based odorant detection system.

Chapter 5.

Optimization of the odorant detection system using CRE reporter system

Chapter 5. Optimization of the odorant detection system using CRE reporter system

5.1 Introduction

In human olfaction, cAMP is produced and works as a secondary messenger via intracellular signaling. Thus, the binding of odorant and receptor can be measured using the reporter system based on cAMP response element. Recently, CRE reporter system has been used in study of receptor or intracellular molecules associated with CRE pathway activation including olfactory receptors. When odorant molecules bind to the olfactory receptor, the cAMP level was increased and initiated the phosphorylation of the CREB which binds to CRE promoter to induce the expression of reporter protein. Many researchers used the luminescence protein as a reporter. In this study, for the visualization of odorant response, the green fluorescence protein ZsGreen was used as a reporter. The original plasmid pcDNA3 was modified to contain the CRE reporter system, and the various number (2, 4, 12) of CRE sites was inserted into the plasmid to enhance the expression level of ZsGreen. And the HEK-293 cell line containing CRE reporter system was constructed. The function of the cell line was tested using forskolin and IBMX was used to enhance the fluorescence level.

Human has about 390 ORs, however, only few ORs were characterized. To characterize the many orphan ORs, and analyze the various odorant binding pattern, there is demand for the development of simple, miniaturized,

economic high-throughput assay platform. In this study, a polyethylene glycol diacrylate (PEG) microwell was fabricated to be used as a miniaturize cell culture platform (Kwon et al., 2011; Moeller et al., 2008). Due to the cell-repellent property of PEG, cells adhere only to the glass bottomed-wells, thus the cells can be seeded as an array type. This method does not require complex chemical treatment or tedious experimental steps. Here, the condition of the fabrication of PEG microwell was optimized and the activity of CRE cell line on the PEG microwell was tested.

5.2 Optimization of CRE reporter system

The CRE-DD-ZsGreen1 genes were amplified from the original vector pCRE-DD-ZsGreen1 and inserted into pcDNA3, which its original promoter was deleted. The pCRE-DD-ZsGreen1 has 2 CRE sites, however, the more CRE sites were added into pcDNA3 vector system. Then, the HEK-293 cells were transfected with pcDNA3-4CRE and pcDNA3-12CRE. The cellular activity in the expression of reporter protein was tested using forskolin. Fig. 5. 1 shows the HEK293 cells expressing ZsGreen1 upon 10 μM forskolin stimulation. The result indicates that the expression level of ZsGreen1 was higher in the cells containing 12 CRE sites than the cells containing 4 CRE sites.

The vector system also contains DD genes, which encodes the destabilizing domain. The DD protein induces the degradation of the linked protein which is expressed from leaky promoters in the absence of shield1. Thus, the shield1

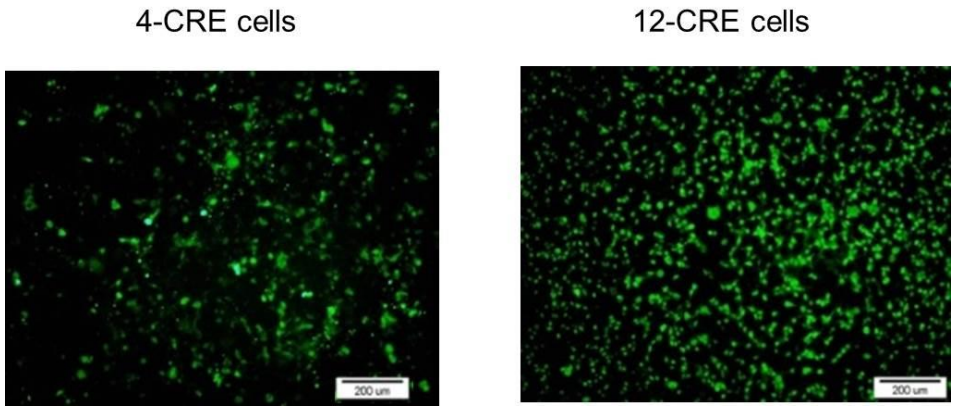

Figure 5.1 HEK-293 cells containing 4 CRE or 12 CRE sites. The expression level of the reporter protein ZsGreen was tested using 10 μM of forskolin. The cells containing 12 CRE sites expressed the ZsGreen in higher level than the cells containing 4 CRE sites. S

hould be added into the medium when the cells are stimulated with the odorants. To optimize the concentration of shield1, various concentration of shield1 was added to the medium and Fig. 5. 2 shows that the 1/1000 shield1 was proper to express the reporter protein.

5.3 Construction of the HEK293-12CRE stable cell line

The HEK293-12CRE stable cell line was constructed, and expression of the reporter protein ZsGreen was confirmed by treatment with 10 μM forskolin and 1 μM Shield-1. Forskolin directly stimulates adenylyl cyclase, which promotes the transformation of ATP to cAMP. The increased cAMP activate protein kinase A (PKA) by phosphorylation and the activated PKA phosphorylates the CRE binding protein (CREB), which binds to the CRE promoter to induce expression of the reporter protein (Redmond et al., 2004; Tian et al., 2007). The Shield-1 efficiently covered the DD fused with the N terminal of the reporter protein ZsGreen, consequently helping expression of the ZsGreen. To increase fluorescence intensity, 100 or 200 μM IBMX was added with or without 10 μM forskolin. IBMX blocks the phosphodiesterase activity which converts cAMP to ATP, resulting in a high level of cAMP. Consequently, the HEK293-12CRE cells treated with IBMX expressed higher levels of ZsGreen under the 10 μM forskolin treatment than cells untreated with IBMX (Fig. 5.3A). Figure 5.3B shows that there was no significant difference in fluorescence intensity between cells treated with 100 or 200 μM.

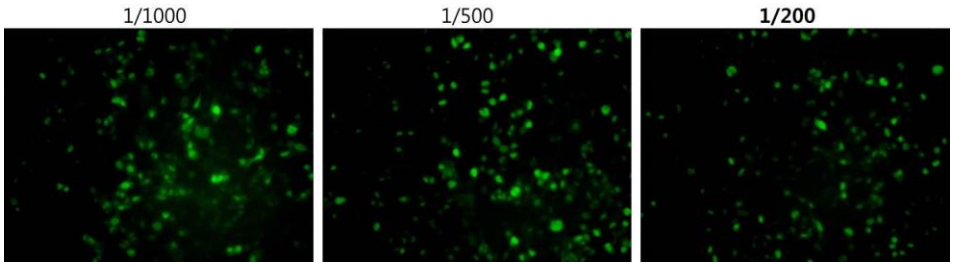

Figure 5.2 The optimization of the concentration of shield1. Cells were stimulated by 10 μM of forskolin with 1/1000, 1/500, and 1/200 of shield1. 1/1000 shield1 was proper to express the reporter protein.

IBMX; therefore, 100 μM IBMX was used for subsequent experiments

5.4 Fabrication of the PEG microwells

The PEGDA solution was prepared by dissolving the PEGDA in DW with the 0.5% (w/w) of the photoinitiator 2-hydroxy-2-methyl propiophenone. The cover glass was treated with TMSPMA for 2 h in 70℃. After washing the glass with ethanol, dry the glass with air pursing. The PEGDA solution was dropped on the TMSPMA-treated glass and pressed with the PDMS stamp. After the UV exposure, the PDMS stamp was peeled off from the glass. Various concentrations of PEGDA (30%, 50%, and 70%) and the various UV exposure time were tested to find an optimized condition for microwell stability. When the microwell was formed using 30% PEGDA for 10 min under UV, it showed good stability compared with that of the other conditions. The microwells made of higher concentrations of PEGDA easily cracked when they were dried at room temperature.

5.5 Cell adhesion on the PEG microwell

An array of 8 × 12 microwells was successfully made on 3-trimethoxysilyl propylmethacrylate (TMSPMA)-treated cover glass (22 × 40 mm) using 30% PEGDA. Fig.5. 4A shows the morphology of the microwell structure observed by scanning electron microscopy. Each microwell had a 500 μm diameter and

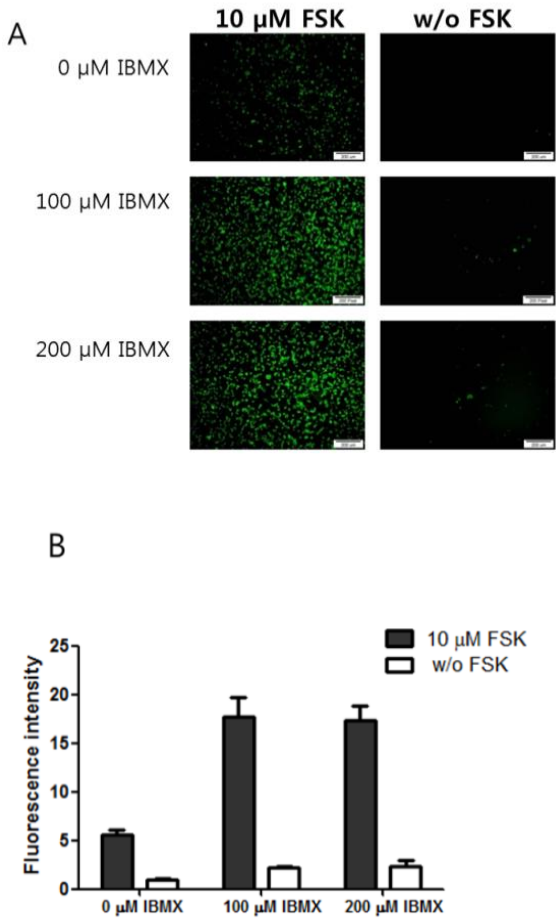

Figure 5.3 Cellular activity of the CRE reporter gene system on the PEG microwell. (A) The function of a constructed HEK293-12CRE cell line was tested using 10 μM forskolin, and 0, 100, or 200 μM IBMX was added to determine the optimum IBMX concentration, which increased fluorescence intensity. (B) As shown in the graph, 100 μM IBMX was sufficient for maximum fluorescence intensity.

100 μm depth. The distance between each well was 1,200 μm. The PEG microwells were stably maintained in culture media for > 5 days, demonstrating that this was a good culture platform for olfactory cell-based odorant screening. Due to the resistant property of PEG to cell adhesion, cells adhered only to the inside of the PEG microwells, which had a glass bottom. After the PEG microwells were sterilized by UV, HEK293 cells were seeded into the microwells. The morphology and number of cells were observed by microscopy 1 day after incubation. As shown in Fig. 5.4B, cell morphology was comparable to that in conventional culture plates. Each microwell contained 300–400 cells.

5.6 Cellular activity in the expression of reporter protein on the PEG microwell

To test the cellular activity of the HEK293-12CRE cell line on the PEG microwells, we cultured the cell line on the microwells, and 10 μM forskolin was added with 1 μM Shield-1 and 100 μM IBMX for 24 h (Fig. 5.5 A and B). These results show that the HEK293-12CRE cells remained stable for expressing ZsGreen on the microwells. We found that the density and cellular activity in each microwell appeared to be fairly consistent. These results suggest that the PEG microwells can be used as a biocompatible and stable platform to conduct a CRE reporter system-related cell-based assay.

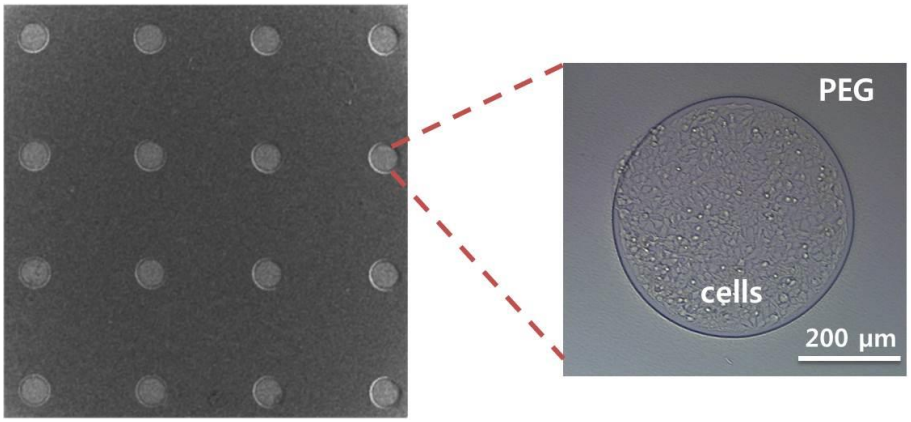

Figure 5.4 Scanning electron microscopic image of the fabricated PEG microwell. The diameter of each well was 500 µm, and the depth was 100 µm. The distance between each well was 1,200 µm. After the cells were seeded, they grew, and 300–400 cells were observed in each well.

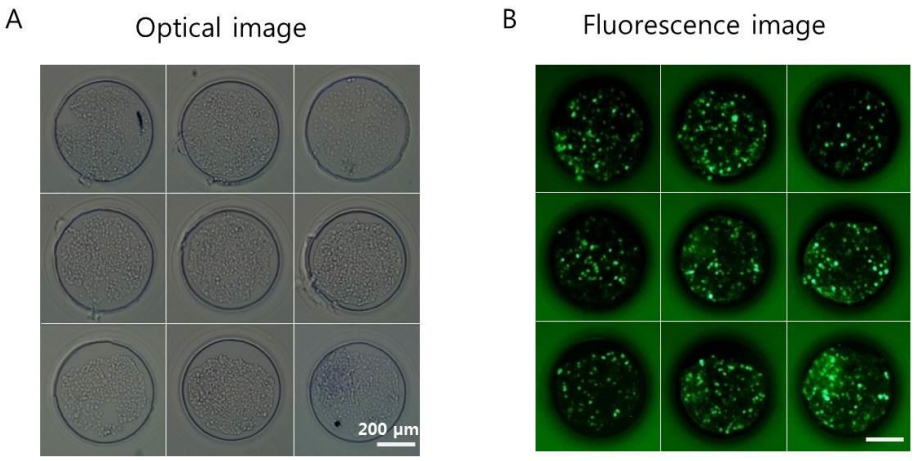

Figure 5.5 Optical (A) and fluorescence (B) image of HEK293 cells containing the CRE reporter gene system on the microwell. The cells were stimulated with 10 μM forskolin together with 100 μM IBMX and 1 μM Shield-1 to express the green fluorescence protein, and they were used as a positive control.

5.7 Conclusions

Recently, various visualizing techniques such as calcium imaging and BRET have been developed for the characterization and patterning of the odorant response. However, the complex experimental steps and too short time response make the system to have a limitation in application of high-throughput odorant detection system. In this study, the HEK-293 cell line containing CRE reporter system was constructed using the fluorescence protein ZsGreen as a reporter protein for visualizing the odorant response of hOR for the high-throughput application. The number of CRE sites and the concentration of IBMX was optimized to enhance the expression of fluorescence protein. And the PEG microwell was constructed using PEGDA solution and PDMS stamp to construct the high-throughput platform. The fabrication condition of the PEG microwell was optimized and the cellular activity of HEK-293 cells containing CRE reporter system was tested using forskoline. As a result, the cells have a good activity in the expression of fluorescence reporter protein on the PEG microwell. This study shows that the PEG microwell combining with CRE reporter cell can be used as an efficient tool for the visualizing of odorant response.

Chapter 6.

Development of high-throughput odorant detection system on the PEG microwell

Chapter 6. Development of high-throughput odorant detection system on the PEG microwell

6.1 Introduction

The development of a cell-based high-throughput screening system has attracted much attention from researchers who study drug screening mechanisms and characterization of G-protein coupled receptors (GPCRs)[119-122]. Although olfactory receptors (ORs) constitute the largest group of GPCRs that play a critical role recognizing and discriminating odorants, only a few ORs have been characterized, and most remain orphan. The conventional cell-based assay system for characterizing GPCRs, including ORs, is very laborious, time consuming, and requires an expensive assay system. In this study, we developed a simple, low-cost miniaturized odorant screening method by combining reverse transfection technology with the Micro-Electro-Mechanical system (MEMs) technique and visualization technique for detecting an odorant response. We fabricated the PEG microwell and applied it to cell culture and a reverse transfection platform for cell-based high-throughput odorant screening. In 2001, Ziauddin and Sabatini developed a new method to conduct cell transfection at the microarray level, which is called reverse transfection technique[123]. By printing various cDNAs onto a slide glass with a transfection reagent followed by seeding of adherent mammalian cells, different proteins can be expressed at each location. It thus became possible to scale down high-throughput gene analysis in a chip-based

system[124-126]. To improve reverse transfection efficiency and to prevent spot-to-spot diffusion, the distance between the different transfection clusters was adjusted and various glass coating materials have been used[127, 128] However, these methods still have a limitation of a high cost coating material and complex experimental steps. . In this study, the PEG microwell was used to generate a spatially separated cell adhesion area[129-133]. For the first time, the reverse transfection was carried out on the PEG microwell and the microwell system effectively avoids cross contamination of DNA spots. In this study, this system was used to express four de-orphaned ORs. The odorant response was detected via fluorescence analysis on the microwell using a CRE reporter assay. This new cell-based screening method not only reduced numerous time-consuming steps but also allowed for simple, efficient, and quantitative screening and patterning of large numbers of GPCRs including ORs, which can help to visualize the OR response to odorants on a microwell.

6.2 Expression of hOR on PEG microwell

6.2.1 Optimization of reverse transfection

For the construction of the high-throughput odorant screening platform, reverse transfection technique was used for the simultaneous expression of various hORs. To optimize the condition for the high efficient reverse transfection, various concentration of the plasmid containing green fluorescence protein (GFP) gene was tested. 0.2% gelatin solution was

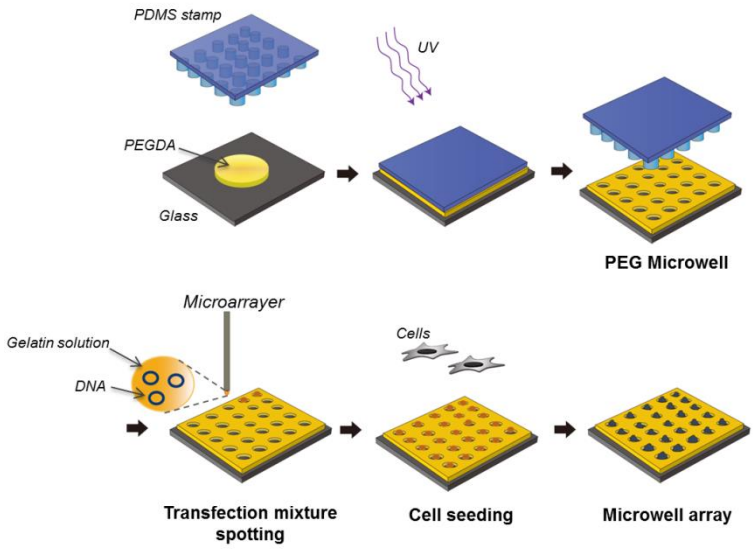

Figure 6.1 Schematic diagram of PEG microwell-based high-throughput odorant screening system. The transfection mixture containing pcDNA3/hOR and the transfection reagent is spotted onto the microwell. After drying the glass, HEK-293 cells containing CRE reporter system are seeded. Different ORs can be expressed on each microwell.

prepared by dissolving the gelatin powder in DW in 50℃ for 20 min. Then, the solution was filtered using 0.2 μm filter. 4 μl of lipofectamine 2000, 4 μl of Opti-MEM and various concentration of the plasmid 100 ng/μl to 500 ng/μl was mixed in 0.2% gelatin solution. The transfection mixture was spotted in the bottom of the cell culture plate and dried for 12 h. Then the HEK-293 cells were seeded on the plate and cultured for 48 h for the expression of GFP. The expression of GFP was detected using fluorescence microscopy. As shown in Fig. 6.2, the fluorescence was highest when 200 ng/μl of the plasmid was used.

6.2.2 Expression of hOR on the PEG microwell using reverse transfection technique

For the high-throughput odorant screening, the PEG microwell array was used as a platform for the reverse transfection. We used two types of mammalian expression vectors expressing EGFP and DsRed to test reverse transfection efficiency on the PEG microwells. Each plasmid was mixed with a transfection mixture containing Opti-MEM, Lipofectamine 2000, and 0.2% gelatin solution. The transfection mixture containing the pEGFP-N1 or pDsRed-N1 plasmid was spotted on the PEG microwells to test whether the plasmids diffused into other wells and did not mix with the plasmids in other spots. The transfection mixture spotted-microwells were dried for 12 h at room temperature. Then, 48 h after HEK293-12CRE cells were seeded on the microwells, the expression of green or red fluorescence protein was observed by fluorescence microscopy. As shown in Fig. 6. 3A, the transfection mixture

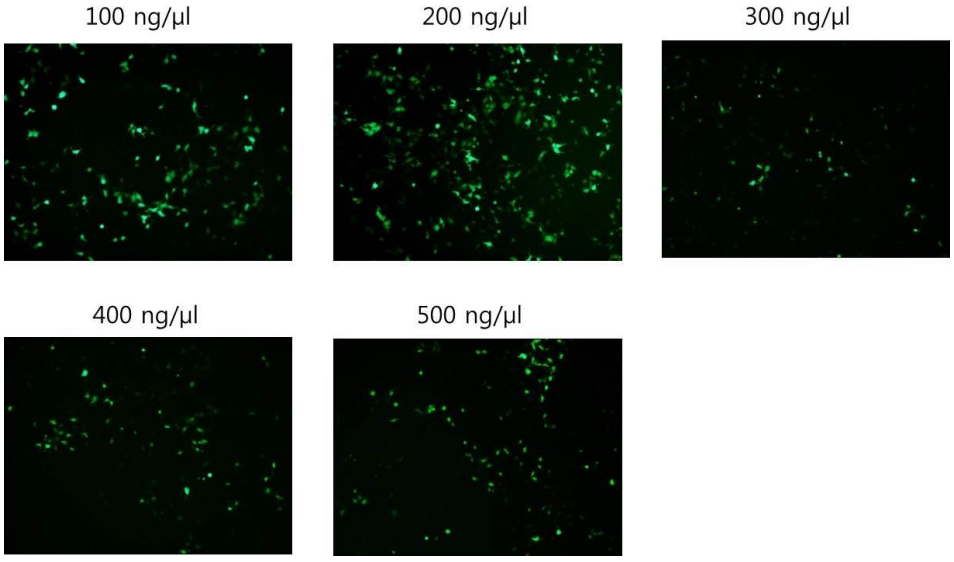

Figure 6.2 Reverse transfection efficiency. Various concentration of plasmid coding GFP were tested to optimize the condition of the reverse transfection. Transfection mixture contains 4 μl of lipofectamine 2000, 4 μl of Opti-MEM and various concentration of the plasmid 100 ng/μl to 500 ng/μl in 0.2% gelatin solution.

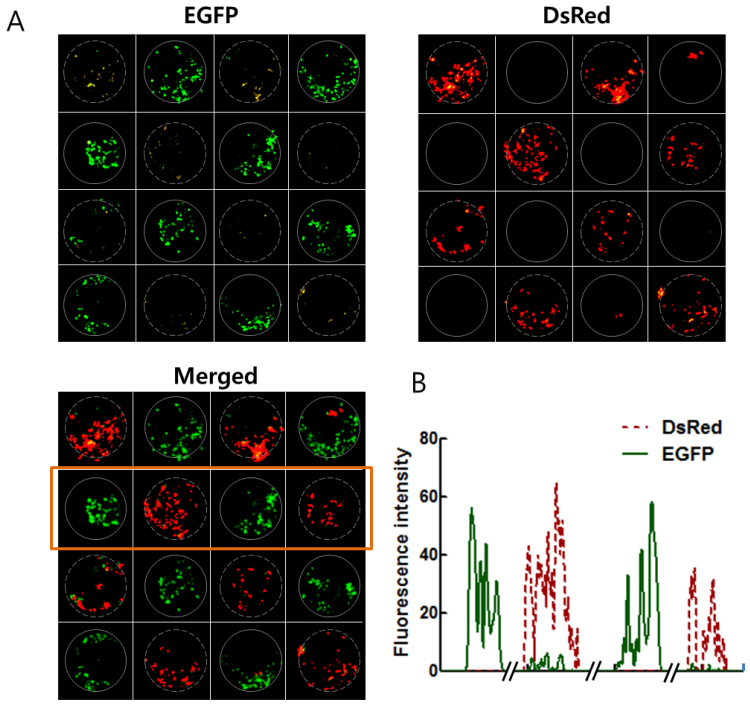

Figure 6.3 Reverse transfection on the PEG microwell. pEGFP-N1 and pDsRed-N1 were used to express the green and red fluorescence proteins, respectively. These two fluorescence proteins were used to examine the cross contamination among neighboring microwells. (A) Transfection mixtures containing 4 μg Opti-MEM/sucrose, 4 μg Lipofectamine, 2 μg 1.2% gelatin solution, and 2 μg of each plasmid were spotted into each microwell. The green and red fluorescence proteins were expressed after a 48 hr culture. The cross contamination of different transfection mixtures was not observed among microwells. (B) The fluorescence intensities of green and red fluorescence are represented by a line plot.

spotted on the wells did not diffuse into other wells, and the green and red fluorescence proteins were expressed with good efficiency. Both green and red fluorescence intensities from each well were calculated using Image J software, and shown as a line plot (Fig. 6.3B). This result indicates that the PEG microwells were an efficient barrier to prevent spot-to-spot diffusion of the transfection mixture.

6.3 Enhancement of OR membrane expression on PEG microwells using RTP1S

Co-expression with RTP1S induces more OR cell-surface expression[62]. To test the effect of RTP1S on the expression level and intracellular signaling of ORs on the PEG microwell system, HEK293-12CRE cells were reversely transfected with both pcDNA3/hOR3A1 and pcDNA3/RTP1S. The $G\alpha_{olf}$ protein was also expressed using pcDNA3.1/$G\alpha_{olf}$ to improve olfactory signaling. As overexpression of the membrane protein might generate cell damage, 4 μL of media containing pcDNA3/hOR3A1 and Lipofectamine 2000 was mixed with or without 0.2 μg pcDNA3/RTP1S. The membrane expression level of the OR protein was detected by an immunocytochemical method. The HEK-293 cells co-transfected with pcDNA3/hOR3A1 and pcDNA3/RTP1S expressed a larger amount of hOR3A1 than cells transfected with only pcDNA3/hOR3A1. Cells transfected with 2 μg pcDNA3/hOR3A1 and 0.2 μg pcDNA3/RTP1S caused 20% higher membrane expression of hOR3A1 than cells transfected with 1.5 μg pcDNA3/hOR3A1 with 0.2 μg

pcDNA3/RTP1S, and no remarkable cell damage was observed under either condition (Fig. 6. 4). Another three ORs, of which specific ligands are known, were used to confirm that the PEG microwell-based system was an effective screening tool. 2 μg of each pcDNA3/hOR with pcDNA3.1/$G_{\alpha olf}$ and pcDNA3/RTP1S was used, and the expression of the proteins was confirmed using an immunocytochemical method (Fig. 6.5).

6.4 Odorant screening by visualization using the CRE reporter system on PEG microwells

The CRE reporter assay system has been used to study cell or protein functions mediated by the cAMP-related pathway. The cellular response induced by ligand-receptor binding can be detected by fluorescent or luminescent reporter gene expression. In this study, ZsGreen, a green fluorescence protein originating from *Zoanthus* sp. was used as the reporter protein. The cellular response induced by odorant-OR binding was visualized by fluorescence imaging using fluorescence microscopy. A reporter gene expression system using a fluorescent protein has several advantages. First, as there is no need to label the protein or to load the dye, many steps affecting the cellular condition can be skipped. Second, fluorescence of the reporter protein is stably maintained for a long time; thus, image capture and analysis using microscopy can be readily conducted. Third, it is possible to compare the responses of different ORs to one odorant simultaneously. To detect the

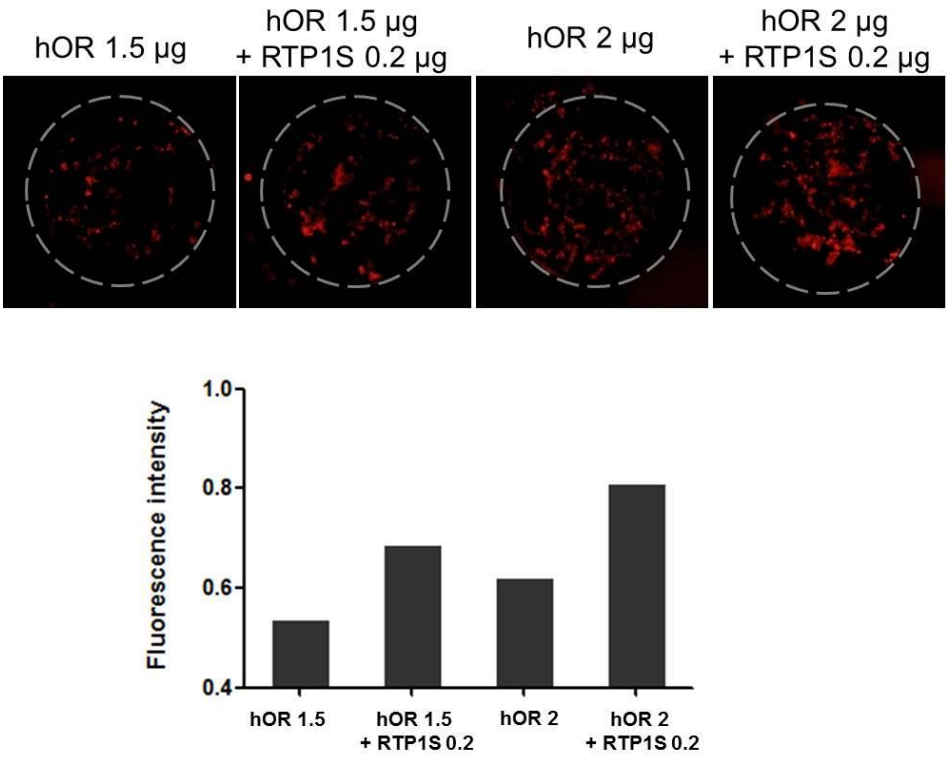

Figure 6.4 Expression of human olfactory receptors on PEG microwells. Reporter transport protein (RTP1S) was tested to enhance overexpression of ORs on the PEG microwells. Because overexpression of ORs in the plasma membrane can be toxic to cells, 1.5 or 2 µg pcDNA3/hOR3A1 was mixed with 0.2 µg pcDNA3/RTP1S. This result demonstrated that RTP1S together with 2 µg pcDNA3/hOR3A1 could be used to enhance OR expression on the microwells without any toxicity.

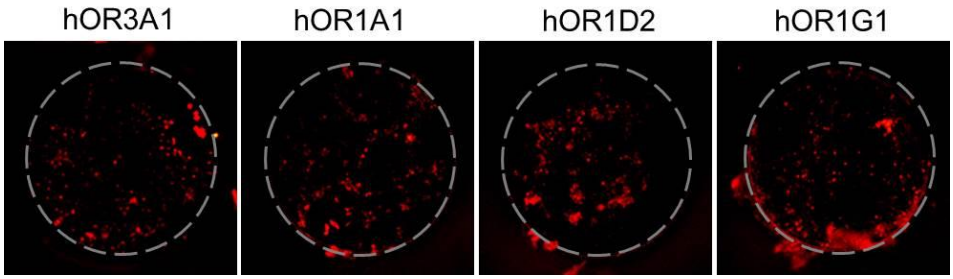

Figure 6.5 Expression of various ORs on PEG microwell. Four different ORs were reversely expressed on the PEG microwells and OR expression was confirmed using immunocytochemistry.

response to an odorant, HEK293-12CREs cells were reversely transfected with four different ORs, hOR3A1, hOR1A1, hOR1D2, and hOR1G1[38, 55, 134], which are known to specifically bind to helional, β-citronellol, bourgeonal, and geraniol, respectively. Each odorant (500 μM) with 100 μM IBMX and 1 μM Shield-1 was added to the transfected HEK293-12CRE cells, and the odorant response was detected by fluorescence microscopy after a 1 day incubation. The negative control was the transfected HEK293-12CRE cells that were not treated with odorant but only with the same concentrations of IBMX and Shield-1. The negative control produced extremely low fluorescence, which was considered a negligible background signal. Figure 6. 6 shows the response of the cells expressing each OR against its ligand. When the cells were stimulated with 500 μM helional, cells expressing hOR3A1 produced the highest fluorescence, whereas cells expressing other receptors showed relatively low fluorescence. Similarly, when the cells were stimulated with 500 μM β-citronellol, bourgeonal, or geraniol, respectively, the cells expressing each counterpart OR showed the highest fluorescence intensity. These results showed that the PEG microwell-based screening system can be used to characterize orphan ORs visually in a high-throughput format.

6.5 Dose-dependent response

We also tested the dose-dependent response of OR to odorant on the PEG microwell-based system using the hOR3A1-expressing cells, from concentration 50 nM to 500 μM of helional. As shown in Fig. 6.7A, the

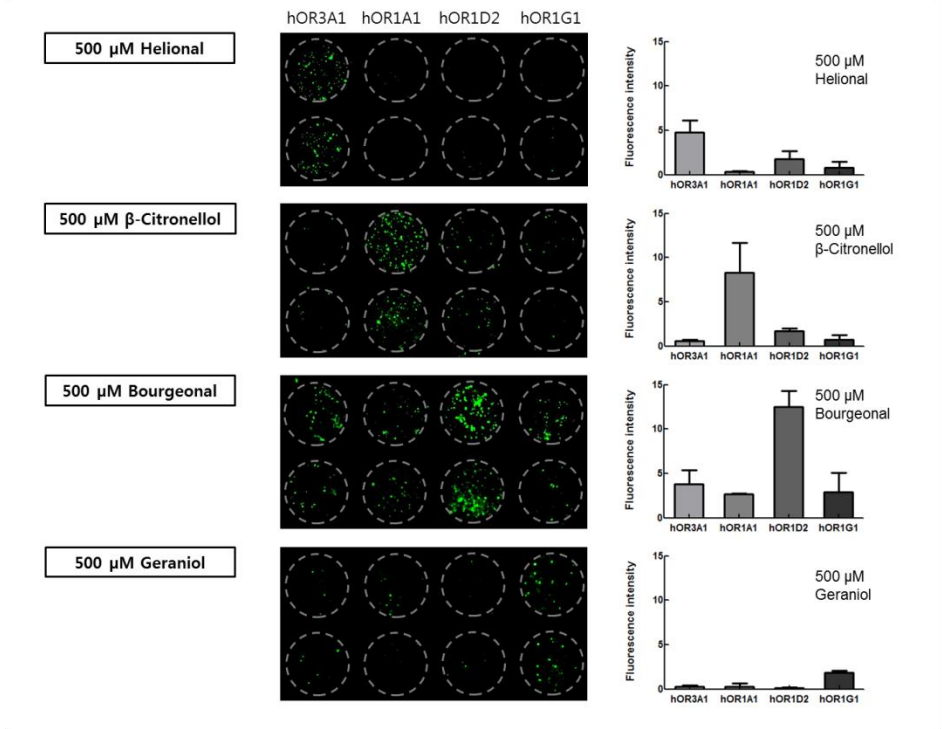

Figure 6.6 Response of ORs to odorants on PEG microwells. Four different ORs, whose specific ligands are known, were chosen for the CRE reporter assay to screen specific odorants on the microwell. The known specific ligands were helional, β-citronellol, bourgeonal, and geraniol for hOR3A1, hOR1A1, hOR1D2, and hOR1G1, respectively. Each ligand (500 μM) together with 100 μM IBMX and 1 μM Shield-1 were injected into the microwells on which four different ORs were expressed. In all four cases, the highest fluorescence intensity was observed when each ligand bound with its counterpart OR.

fluorescence increased with helional concentration. The fluorescence intensity of each well was calculated using Image J software and plotted in Fig. 6 .7B. The EC_{50} value was 9.6 ± 1.7 μM which is 10 fold lower than the conventional calcium detection method[135]. Thus, this PEG microwell-based odorant screening system is useful not only for the qualitative analysis but also for the quantitative analysis. Humans recognize and discriminate smells through a combination of responses to individual odorants. If a smell is visualized by developing a map of each smell, the visualized image can be used as a code for each smell. The PEG microwell array system proposed in this study provides a tool to visualize smells. Using this approach, smell can be categorized and systematically classified, and a sensory evaluation of smell can be replaced with instrumental analysis. If this approach is combined with a microchip system, it will be further miniaturized and more powerful for the high-throughput odorant pattern detection system. Therefore, this technique would fundamentally contribute to change this area from art to science.

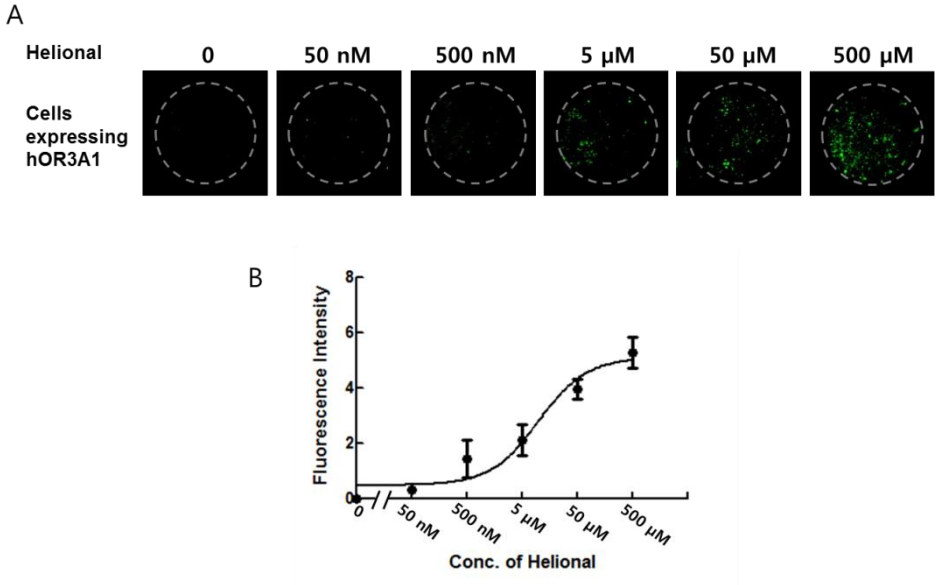

Figure 6.7 Dose-dependent response of OR to odorant. (A) hOR3A1-expressing cells were stimulated with 50 nM to 500 µM of helional with 100 µM IBMX and 1 µM Shield-1. The fluorescence increased with the concentration of helional. (B) The fluorescence intensity of each well was calculated using Image J software and shown as line plot. The EC_{50} value was 9.6 ± 1.7 µM.

6.6 Conclusions

We applied the PEG microwell system combined with the reverse transfection technique for the construction of simple, miniaturized, and high-throughput OR screening platform. Various ORs were expressed simultaneously on the PEG microwell using reverse transfection. The odorant response was visualized by the fluorescence pattern on the microwell. This new approach of the odorant detection provides important potential advantages over the conventional odorant screening system. First, cells can be cultured and transfected on a small-sized well providing an inexpensive and efficient culture environment for cellular assays. Second, because the OR gene printed-PEG microwell is highly stable, it can be fabricated in large quantity and can be stably stored for odorant screening. Thus, there is no need to conduct transfection of cells with OR genes every time before seeding the cell on the microwell. Finally, various OR responses to the specific odorant can be visualized simultaneously and patterned on miniaturized platform demonstrating its applicability to the medical, biological, and industrial fields.

Chapter 7.

Ion channel-coupled OR for real time visualization of odorant response

Chapter 7. Ion channel-coupled OR for real time visualization of odorant response

7.1 Introduction

In a human smell sensing system, there are about 390 kinds of olfactory receptors (ORs), which bind to various odorants with different affinity and specificity. The characterization and the odorant binding pattern analysis of OR are essential to understand human olfaction and to mimic the olfactory system for various applications. Although the various cell-based odorant screening systems have been developed for this purpose, many of human ORs (hORs) still remain orphan because of the time-consuming and labor-intensive experimental procedures of the screening methods. In the previous study, we constructed the odorant screening platform for the high-throughput odorant screening and the pattern analysis of odorant binding by visualizing the odorant response. The odorant response of various ORs was visualized by the imaging the green fluorescence generated from the reporter protein on the poly ethylene glycol (PEG) microwell platform. The study showed potential advantages for the visualization of odorant response as well as the high-throughput odorant screening. However, the detection using the fluorescence protein needs the protein expression time, at least few hours. Thus, the odorant response cannot be immediately detected or visualized. To overcome this limitation, we constructed a new odorant sensing system by coupling of ion channel to olfactory receptor for the fast visualization of odorant response.

In this study, we constructed the ion channel-coupled hOR for the simple odorant detection by visualizing the odorant response in real time to overcome the limitation of the conventional screening system. The hORs were coupled to the potassium channel Kir6.2[107, 135]. The channel protein Kir6.2 is the subunit of the ATP-sensitive potassium channel and four Kir6.2 form K^+-selective pore[136, 137]. The hOR-Kir6.2 fusion proteins were expressed in HEK293 cells. When the odorant binds to the hOR coupled to the ion channel, the odorant binding causes the conformational change of OR, and this consequently opens the ion channel, resulting in the ion influx into the cell. Then this ion influx was visualized using a membrane potential dye. Cells expressing ion channel coupled-hOR showed the high sensitivity and selectivity to their specific odorant and also the odorant-hOR binding pattern was visualized for identifying the response of individual hOR to various odorants as well as the response of various hORs to various odorants. These results indicate that the ion channel-coupled hOR can be effectively used not only for a simple and fast high-throughput odorant screening but also for the visualization of odorant-hOR response pattern.

7.2 Construction of the ion channel-coupled hOR

The construction of M_2 and D_2 ICCRs, which was reported in 2008, was used as a model system to construct the ion channel-coupled OR. These two receptors were coupled to a Kir6.2 deleting various numbers of amino acid sequences at N-terminal of genes, and the receptors, which were coupled with

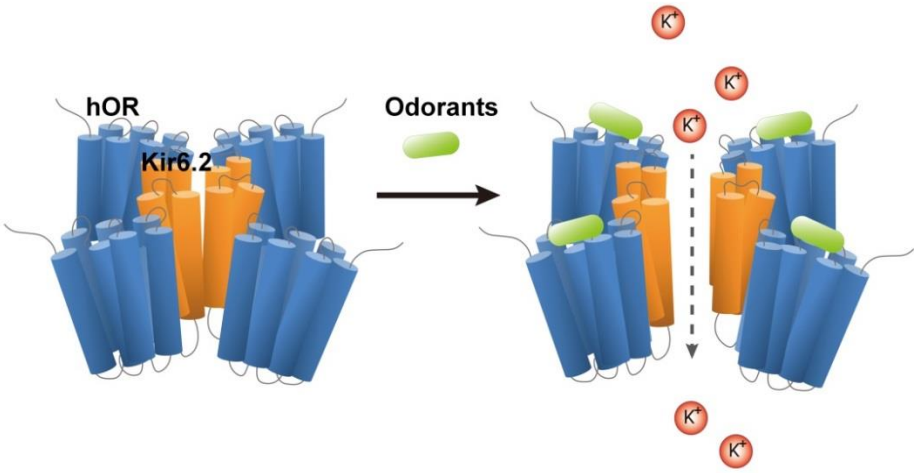

Figure 7.1 Principle of ion channel-coupled human olfactory receptor. Four hOR-K forms the one ion channel. When the odorant binds to the hOR part of hOR-K, the conformational change of hOR induces the linked ion channel Kir6.2. to open. The potassium ion flows into the cell via the channel.

Kir6.2 lacking its first 25 amino acids showed the highest membrane potential changes upon ligand stimulation. Olfactory receptor, belonging to G-protein coupled receptor family, has a similar functional structure with the M_2 and D_2 receptor. Therefore, we adopted this concept to the four different human olfactory receptor hOR2AG1, hOR1A2, hOR3A1, and hOR1G1, which are well-known to bind with amylbutyrate, β-citronellal, helional and 1-nonanol respectively. The ion channel-coupled hORs were constructed by coupling the hORs with a truncated Kir6.2 lacking its first 25 amino acids. The hOR-Ks were designated by hOR2AG1-K, hOR1A2-K, hOR3A1-K and hOR1G1-K (Fig. 7.1). We also constructed hOR2AG1-(6G)-K by the addition of the hexaglycine linker between the hOR2AG1 and Kir6.2 to test the effect of the linker on the enhancement of hOR-Ks performance. To enhance the expression of the receptor in the cell membrane, the rho-tag sequence was inserted at the N-terminus of hOR gene.

7.3 Expression of ion channel-coupled hOR

The hOR2AG1 and the ion channel-coupled hOR2AG1 were expressed in HEK-293 cells and the expression was confirmed by the immunocytochemical method and the Western blot using anti-rho antibody as shown in Fig. 7. 2A and B. The OR protein and the hOR-K protein were expressed in the cellular membrane and the band of each protein was observed in the proper size. The four different hOR-Ks (hOR2AG1-K, hOR1A2-K, hOR3A1-K, and hOR1G1-K) were also expressed in HEK-293 cells and the

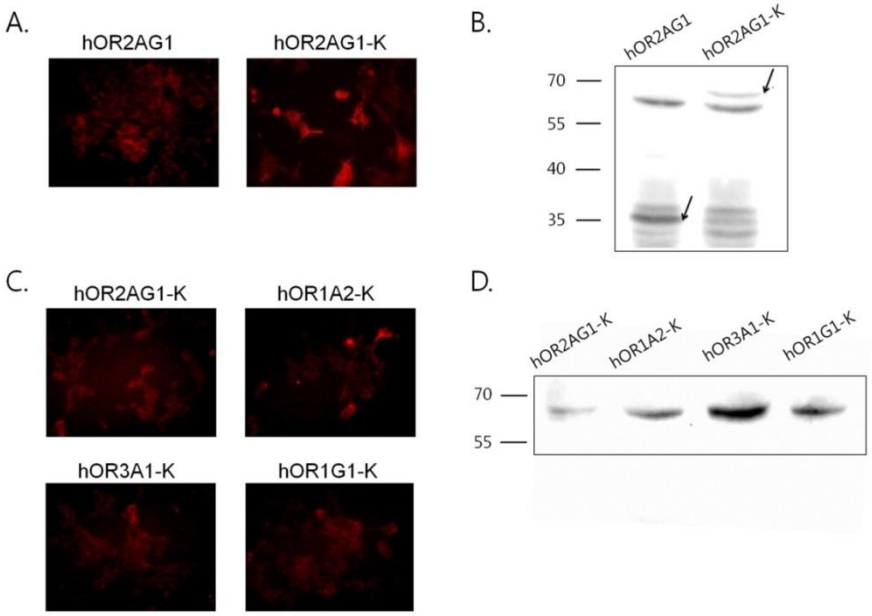

Figure 7.2 Immunocytochemistry and Western blot images. A, B) hOR2AG1 and hOR2AG1-K. (primary Ab: anti-rho Ab, secondary Ab: HRP-conjugated anti-rabbit Ab) C, D) Four different hOR-Ks (hOR2AG1-K, hOR1A2-K, hOR3A1-K, and hOR1G1-K). The primary Ab for Western blot was anti-Kir6.2 Ab, and the secondary Ab was HRP-conjugated anti-rabbit Ab.

expression was confirmed by the immunocytochemical method and the Western blot using anti-Kir6.2 antibody as shown in Fig. 7.2C and D.

7.4 Functional analysis of the ion channel-coupled hOR

The function of hOR-Ks was analyzed using FLIPR membrane potential dye and spectrofluorometer. The fluorescence change of the membrane potential dye indicates the influx or the outflux of the positively charged ions. The fluorescence intensity increases during as the positively charged ions flow into the cells, and the fluorescence intensity decreases as the positively charged ions flow out from the cells. It was expected that when the odorant binds to the hOR-K, the conformational change of the olfactory receptor induces the linked potassium ion channel Kir6.2 to open resulting in the influx of potassium ions into cells. When the cells expressing hOR2AG1-K was stimulated by with the 20 μM of amylbutyrate, the fluorescence intensity increased, while the stimulation of cells by DW, which was used as a control, showed slight change of fluorescence intensity (Fig. 7.4A). This result indicates that the ion influx was generated upon the ligand stimulation. However, it was considered that the increase in fluorescence intensity have included the increase amount by the calcium influx which is originally induced by cAMP-mediated signaling cascade of OR. We tested the ion influx of hOR-K upon ligand stimulation using the well-known calcium channel blocker $MgCl_2$. As shown in Fig. 7.4B, even when 20 μM of amylbutyrate was added with 5 mM of $MgCl_2$ to the cells expressing hOR2AG1-K, the

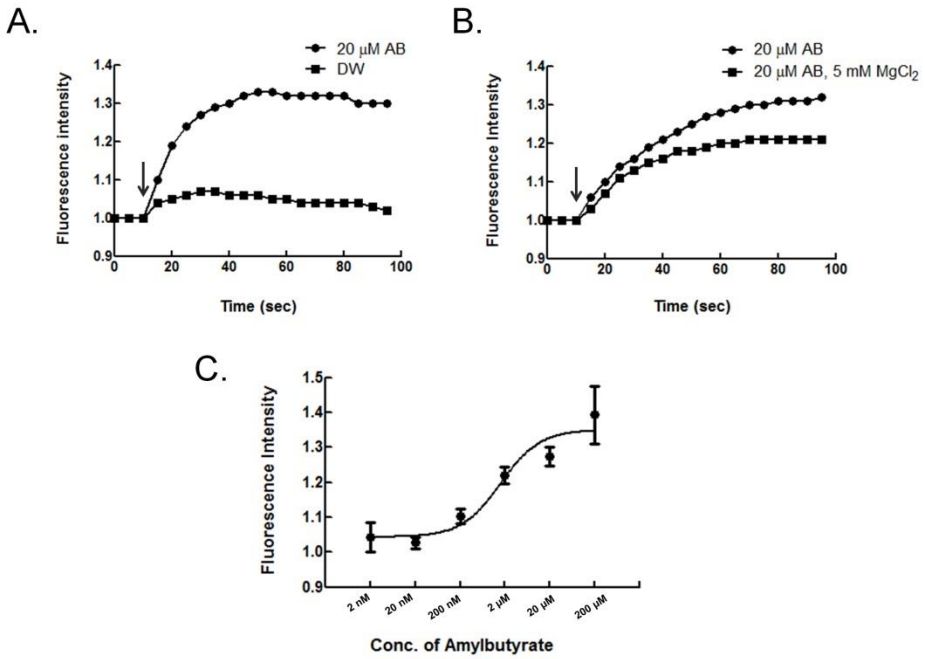

Figure 7.4 The functional analysis of hOR2AG1-K using spectrofluoromer. (A) Stimulation of cells expressing hOR2AG1-K with 20 μM of amylbutyrate (AB) or DW as a control. (B) Stimulation of cells expressing hOR2AG1-K with 20 μM of AB with or without $MgCl_2$, which is known calcium channel blocker. (C) Dose-dependent response of the cells expressing hOR2AG1-K to various concentration of AB. The EC_{50} value was 1.5 ± 0.2 μM

increase in fluorescence intensity was slightly attenuated. This result confirmed the potassium ions flow into the cells through linked potassium ion channel when the hOR2AG1-K binds to the amylbutyrate and most increase in fluorescenc intensity occurred by potassium ion influx. Fig. 7.4.1C shows the dose-dependent response of hOR2AG1-K for various concentration of amylbutyrate from 2 nM to 200 μM. The EC_{50} value was 1.5 ± 0.2 μM which is about 60 fold lower than the conventional calcium imaging method[40]. The addition of hexaglycine linker between hOR2AG1 and Kir6.2 didn't enhance the potassium influx upon ligand stimulation as shown in Fig. 7.5. Thus we used hOR2AG1-K for ligand detection in further study.

7.5 Visualization of odorant response using fluorescence image scanning

To visualize the olfactory response to odorant, the fluorescence was captured by fluorescence image scanner before and after the ligand stimulation. The spectrofluorometer results showed that the increased fluorescence was saturated 80 s after ligand addition. Thus the fluorescence image was captured at the saturation stage after the cells were stimulated with ligand. When the cells expressing hOR2AG1 or hOR2AG1-K were stimulated with 2 nM to 200 μM of amybutyrate, the fluorescence intensity increased along with the concentration of amylbutyrate in both case. However, the cells expressing hOR2AG1-K showed the higher response at the same

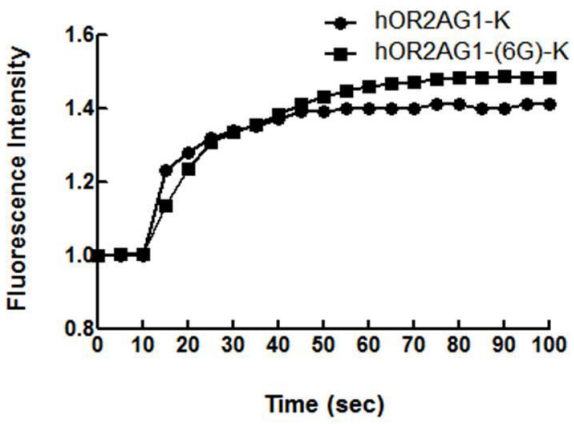

Figure 7.5 Effect of hexaglycine linker between hOR2AG1 and Kir6.2. The linker didn't enhance the function of hOR2AG1-K upon odorant stimulation.

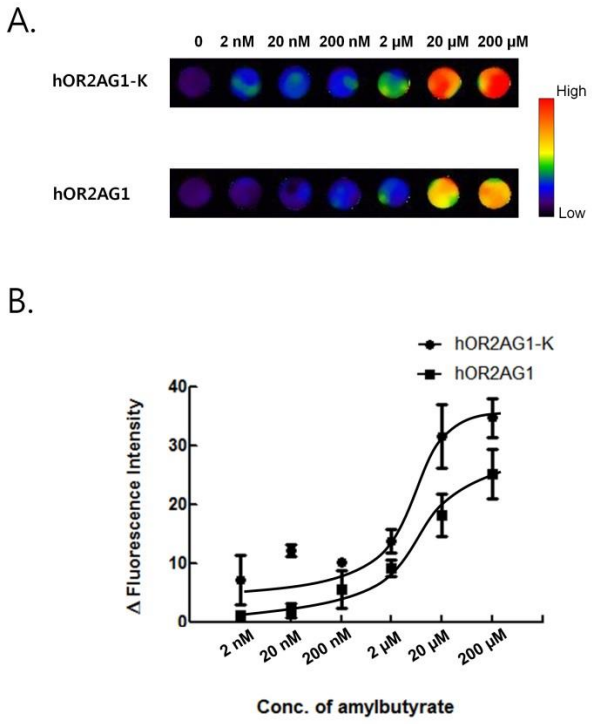

Figure 7.6 Visualization of odorant response of hOR2AG1-K using fluorescence image scanning. (A) Response image of cells expressing hOR2AG1-K or hOR2AG1 to various concentration of AB was presented by pseudo color. (B) Dose-dependent curve of the calculated fluorescence intensity from the odorant response images.

concentration of amylbutyrate than the cells expressing hOR2AG1 at the same concentration of amylbutyrate. Only in the case of hOR2AG1-K, the increase in fluorescence was detected at 2 nM of amylbutyrate (Fig. 7.6). Compared with hOR2AG1, the hOR2AG1-K generated higher fluorescence change due to the potassium influx through linked ion channel in addition to calcium influx.

7.6 Visualized response image to various odorants

In order to visualize the response of the hOR-K to various odorants, the cells expressing hOR2AG1-K were stimulated with 16 different odorants having various functional groups (Fig. 7.7A, B). 200 μM of each odorant was added to the cells and the odorant response was detected by fluorescence image scanning. As shown in Fig. 7.7A, the hOR2AG1-K was very specific to amylbutyrate(component 1) among the similar butyrate compounds (component 1, 2, 3 and 4). However, interestingly it showed a high response to 2-methylpyrazine (component 6), which has a very different chemical structure from amylbutyrate. Due to this characteristic of OR in that various odorant molecules can bind to a single OR, human recognizes and discriminates thousands of odorant molecules from about 390 ORs by combinations of various OR-odorant bindings. The image analysis of the odorant response of hOR2AG1-K using membrane potential dye showed not only the selectivity but also the odorant binding pattern. The fluorescence intensity was measured from the image scanning data using image J software

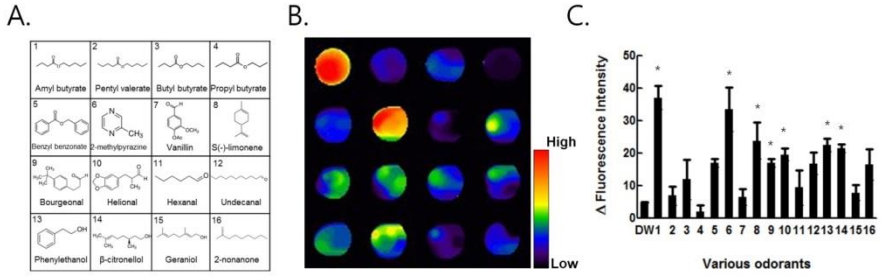

Figure 7.7 Various odorant response of hOR2AG1-K. (A) Chemical structures of the various odorants. (B) Visualized odorant response of hOR2AG-1 to various odorants (C) A bar graph of the fluorescence intensity measured from the image scanning data.

and plotted as a bar graph in Fig. 7.7C. As shown in Fig. 7.7, the response of hOR2AG1-K to various odorants was diverse. Cells expressing hOR2AG1-K barely responded to other odorants which have similar chemical structure with amylbutyrate such as pentyl valerate, butyl butyrate and propyl butyrate, but the cells highly responded to 2-methylpyrazine even though the chemical structure is considerably different from amylbutyrate. These results show that the various odorant response of OR can be visualized simultaneously by the construction of hOR-K and this approach can be used for the high-throughput analysis of odorant binding pattern of a specific OR.

7.7 Visualized response of various hOR-Ks to various odorants

With this method, the odorant can be detected in real time and the odorant response pattern of various ORs can be visualized. In order to visualize the responses of various hORs to various odorants, three more ORs (hOR1A2, hOR3A1, and hOR1G1) were coupled to Kir6.2 by molecular cloning technique. Each ORs are known to bind to β-citronellol, helional and geraniol respectively. Thus, four hOR-Ks including hOR2AG1 were used as sensing materials to visualize the odorant binding pattern. The HEK-293 cells were transfected with four hOR-Ks and the expression was confirmed by Western blot analysis using anti-Kir6.2 antibody. The cells expressing each hOR-K were seeded to 96 well-plate and stimulated with 200 μM of the four different odorant simultaneously and the responses were detected by fluorescence

image scanning. Fig. 7. 8A shows the odorant binding pattern of each hOR-K and the fluorescence intensity was calculated using ImageJ and plotted as a bar graph in Fig. 7. 8B. When the cells expressing four different hOR-Ks were stimulated with amylbutyrate, the cells expressing hOR2AG1-K most highly responded than the cells expressing other hOR-Ks. Similarly, when the cells were stimulated with β-citronellol, helional and geraniol, respectively, the cells expressing each counterpart OR showed the relatively the highest response. Interestingly, hOR2AG1-K the most highly responded to amylbutyrate but barely responded to other odorants, while hOR1A2-K, hOR3A1-K, and hOR1G1-K also highly responded to more than two odorants. And all four hOR-Ks responded to amylbutyrate, while only hOR1G1-K responded to 1-nonanal. To test the effect of amybutyrate on the cells, we stimulated the cells not expressing hORs with 200 μM of amylbutyrate, but the cells did not response to it. Thus, it is verified that all four hOR-Ks bind to amylbutyrate.

These results shows that the various odorant response of various ORs can be visualized as fluorescence intensity by the adoption of the concept of the ion channel coupling with OR and the fluorescence detection using membrane potential dye.

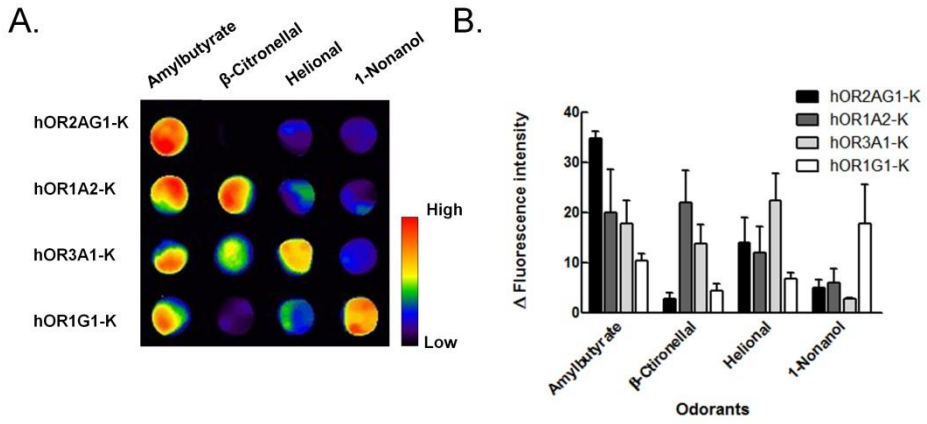

Figure 7.8 Response of various olfactory receptors to odorants. (A) Odorant response pattern of four different hOR-Ks (hOR2AG1-K, hOR1A2-K, hOR3A1-K, and hOR1G1-K) to various odorants. (B) A bar graph of the fluorescence intensity measured from the image scanning data.

7.8 Conclusions

The hOR-K has several advantages to be used as a sensing molecule for odorant detection. First, the sensitivity of odorant detection can be enhanced by the generating large potassium influx via the coupled ion channel. Because the large signal generated by potassium ion influx is added to the signal generated by calcium influx, the odorant detection can be conducted in the lower concentration of odorant than the odorant detection depending only on the intracellular calcium signaling pathway. Second, the various odorant-hOR-K binding patterns can be visualized in real time using membrane potential dye. Unlike other odorant detection system using reporter protein, the odorant responses of various ORs can be detected in real time. Thus the pattern analysis of odorant response can be generated in very short time. We suggest that if we apply the hOR-K to more varieties of ORs, the high-throughput odorant detection and visualization can be carried out. And this system will be useful to characterize the many orphan ORs and to analyze the visualized odorant binding patterns of odorants. Finally, since the hOR-K detection system uses the conformational change of the physically linked-protein rather than intracellular signal transduction reaction, the hOR-K can be effectively used as a sensing material in protein-based odorant detection. The conventional odorant detection system such as calcium detection and CRE reporter system are based on the cellular signaling cascade, thus they are mostly affected by the cellular condition. However, the odorant binding with the hOR-K is rarely affected by cellular condition because it is mainly

operated by the physical conformational change. Thus the odorant can be detected even when the cells are exposed to the unfavorable environmental conditions. Moreover, hOR-K can be applied to more stable and high sensitive protein- or nanovesicle-based olfactory biosensor, which would be combined with various secondary transducers such as FET and electrode. In summary, we report the development of an odorant detection system using hOR-K. The ion channel Kir6.2 was coupled to the various ORs, and the fusion protein was expressed in the HEK-293 cells. The function of hOR-K was analyzed by measuring the fluorescence signal of the membrane potential dye. The hOR-K responded to the odorant with high sensitivity and selectivity. And the binding patterns of various odorants and olfactory receptors were visualized in real time. Our results suggest that the odorant detection system using hOR-K also can be applied to other sensor system to enhance the stability and sensitivity for odorant detection.

Chapter 8.

Visualization of odorant response in gas phase using microfluidic system

Chapter 8. Visualization of odorant response in gas phase using microfluidic system

8.1 Introduction

Many researchers have been interested in developing the odorant detection system using the artificial olfactory cell. In mammalian cell-based system, various signal detection methods using intracellular mechanism have been used for odorant detection. Among them, the detection of calcium influx is the most conventional method. However, until now, the cell-based odorant detection was mostly conducted in liquid phase. However, the odorant detection in gaseous phase is important to be applied to the medical and industrial area by mimicking the human olfactory system. In this study, the cell-based odorant detection system in gaseous phase using microfluidic system was developed. The HEK-293 cells expressing the three different hORs were cultured on the polycarbonate membrane, respectively, and the each membrane was placed in inverted format between the top and bottom PDMS chamber. The three hOR, which are hOR1A1, hOR1D2 and hOR1G1, were known to bind their specific ligand β-citronellol, bourgeonal and geraniol, respectively. The gaseous odorants were injected into the inlet of the top chamber and the response of cells was detected by calcium indicator fluo-4 using fluorescence microscopy. When the cells were exposed to the various concentration of odorant, the cells responded in dose-dependent manner. Also the cells expressing each hOR show the high specificity to their ligand

odorant. Consequently, the microfluidic-based odorant system can be an effective tool to detect the odorant in gas phase and can be used in industrial and medical applications.

8.2 Cell adhesion on the polycarbonate membrane

One of the major issues of our system is that the cells should be cultured on the PC membrane. The cells should be brought up to the membrane without escaping through the pore, and the gaseous odorant molecules can be passed through the membrane pore without a pressure drop. For these reasons, the 2 μm-pore-sized PC membrane was chosen. Furthermore, to optimize the cell culture system, we compared several PC membrane coating methods to determine the most suitable method to culture the cell for the odorant detection. Because the morphology of the cells on the PC membrane was invisible under the bright field microscopy mode, the HEK-293 cells were transfected with the plasmid containing green fluorescence protein (GFP) gene. After the cells were cultured on the coated membrane for 48 h, they were observed using fluorescence microscopy. First, in the control experiment, when the cells were cultured on the bare PC membrane, the cells were partially attached to the membrane (Fig. 8. 1A). Next, when the cells were cultured on the 0.2% gelatin-treated membrane, cells also partially adhered on the PC membrane, even though the gelatin coating is a well-established coating method for a dish or plate (Fig. 8. 1B). When the cells were culture on the 0.1 mg/mL poly-D-lysine (PDL)-treated membrane, the cells adhered on it

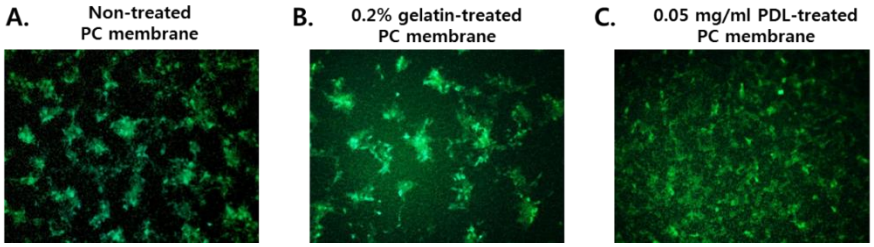

Figure 8.1 Fluorescence image of the cells on the PC membrane with different pre-coating methods. (A) The PC membrane was not treated and used for the cell culture. The cells partially adhered to the membrane. (B) The PC membrane was pre-coated with 0.2 % gelatin for 1 hr. Then the cells partially adhered to the membrane. (C) The membrane was pre-coated with 0.05 mg/mL poly-D-lysine. The cells adhered to and grew uniformly through the overall membrane.

well and grew uniformly on the PC membrane. However, due to the toxic effect of PDL, 0.05 mg/mL of PDL membrane pre-coating shows better results with respect to cell adhesion and growth on the PC membrane (Figure 8. 1C). These results suggest that the 0.05 mg/mL of PDL pre-coating of the membrane is the most suitable for cell culture to monitor the response of cells to gaseous odorants.

For further study, the cells transfected with hOR genes (hOR1D2, hOR1A1, and hOR1G1), and the expression of hORs were confirmed by immunocytochemical method using anti-rho antibody. Fig. 8.2 shows that the hORs were expressed well in the membrane of cells.

8.3 Time-dependent response of cells to gaseous odorant

To monitor the odorant binding response of cells expressing OR to the gaseous odorants, cells expressing hOR1D2 were cultured on a PDL-coated PC membrane. After flou-4 was loaded into the cells, the membrane was placed in the inverted format between the top and bottom PDMS layers. Then, the 200 ppm of bourgeonal was injected into the cells through the inlet tubing. The time-dependent response of the cells was observed using the fluorescence microscopy. The real-time fluorescence images of the cells at different times are shown in Fig. 8.3. When the cells expressing hOR1D2 were stimulated with the gaseous bourgeonal, the fluorescence signal of the cells became stronger along with the stimulation time. After 60 s, the fluorescence intensity

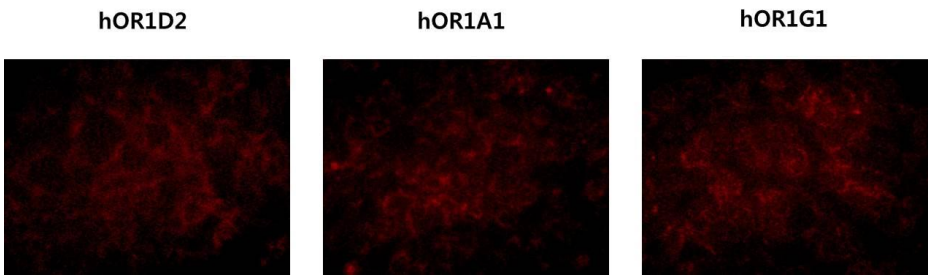

Figure 8.2 Expression of ORs in HEK-293 cells. Anti-rho antibody (1: 500 in PBS containing 1 % BSA) was used as a primary antibody, and anti-rabbit antibody was used as a sencondary antibody (1: 1000 in PBS containing 5 % BSA).

started to saturate, so we decided to capture the odorant response image at 60 s, when the saturation time for further study. The results show that the gaseous odorant molecules bound to the OR on the cell surface through the pore of the PC membrane.

8.4 Dose-dependent response

We investigated the dose-dependent response of the cells expressing OR by stimulation with various concentrations of gaseous odorant molecules. Three different olfactory receptors, hOR1D2, hOR1A1, and hOR1G1, which are known to specifically bind to bourgeonal, β-citronellol, and geraniol, respectively, were expressed in HEK-293 cell. Also, the odorants are well-known to carry the scents of flowers such as of the lily (bourgeonal) and the rose (β-citronellol, and geraniol). The cells transfected with the three hOR genes were cultured on the PC membrane for 48 h to express hOR proteins. Then after fluo-4 was loaded onto the cells, the membrane and the device were assembled. The gaseous odorants were prepared at concentrations of 20, 50, 100, and 200 ppm of bourgeonal, β-citronellol, and geraniol, respectively. The various concentration of gaseous odorants were injected to the counterpart OR, and the change in the fluorescence signal was observed after 60 s. When each OR was stimulated with the counterpart gaseous odorants, the fluorescence signal of the cells increased as the concentration of the gaseous odorants was increased as shown in Fig. 8.4A. The fluorescence signals of the cells were analyzed using ImageJ software and were plotted in

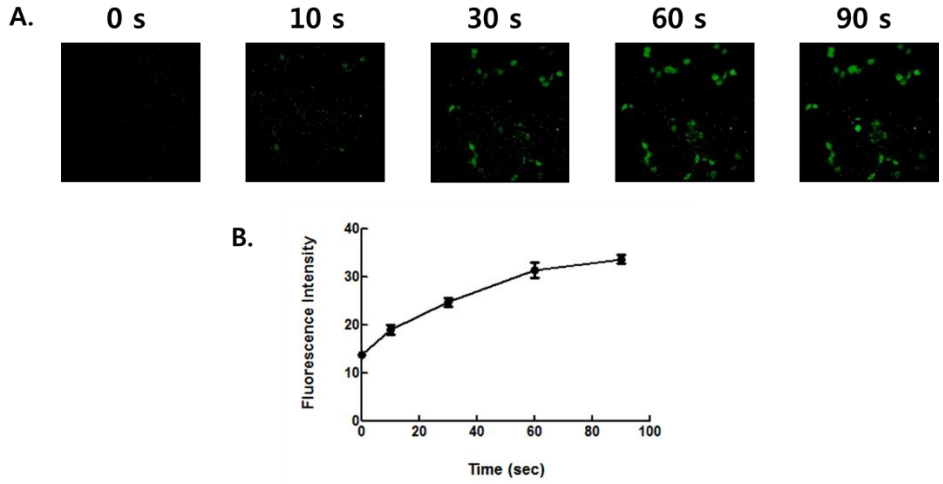

Figure 8.3 Real-time monitoring of the cellular response to the gaseous odorant stimulation. After the cells that expressed hOR1D2 were stimulated with 200 ppm of gaseous bourgeonal, the fluorescence signal was monitored. (A) Real-time fluorescent images of the cells at different times. (B) The fluorescence image was analyzed using imageJ software. As time passed, the fluorescence signal increased.

Fig. 8.4B. The dose-dependent response was observed from 20 ppm to 200 ppm. These results show that the introduction of Ca^{2+} into the cells increased by following the cAMP pathway as the concentration of the gaseous odorant molecules increased. Therefore, based on these results, the gaseous molecules were visualized by our cell-based gas detection system.

8.5 Selectivity test

To test the selective response of the cells expressing OR to gaseous odorants, the each cells expressing hOR1D2, hOR1A1, or hOR1G1 on the PC membrane exposed to the three odorants bourgeonal, β-citronellol, and geraniol. After fluo-4 was loaded into the cells, the device was prepared. The 200 ppm of the gaseous odorant molecules were injected through the inlet for 60 s to the cells and the change in the fluorescence signal of the cells was observed. When the cells expressing hOR1D2 were stimulated with 200 ppm of bourgeonal, a dramatic change in fluorescence signal was observed; however, when the cells were treated with 200 ppm of β-citronellol or geraniol, the change in fluorescence signal became negligible (Fig. 8.5). Similarly, the cells expressing hOR1A1 and hOR1G1 responded to their specific odorant higher than other odorants. These results showed that the system can discriminate the specific gaseous odorant molecules and visualize them using the change in the fluorescence signal. The human nose can discriminate and recognize a gaseous smell. However, because the gaseous smell is invisible, visualization is important as a sensor for diverse purposes

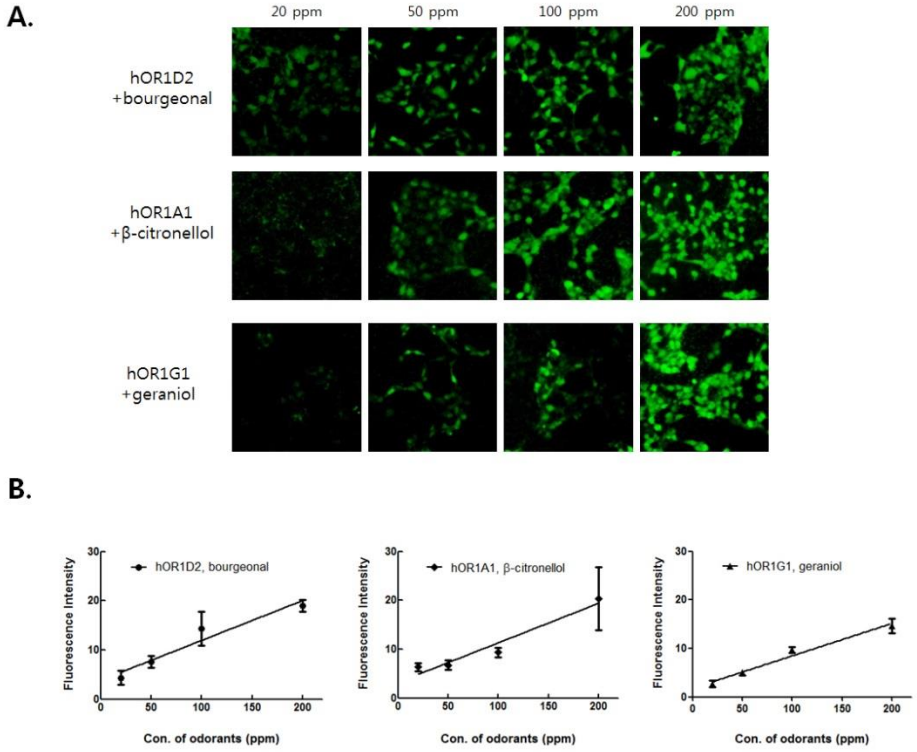

Figure 8.4 Dose-dependent response of the OR to the gaseous odorant molecules. (A) hOR1D2, hOR1A1, and hOR1G1 expressing-cells were stimulated with 20-200 ppm of bourgeonal, β-citronellol, and geraniol, respectively. The fluorescence signals of the cells increased as the concentrations of the gaseous odorant molecules were increased. (B) Concentration-dependent response lines of the OR-expressing cells.

such as safety, fragrance, and flavor. Our system proposed the visualization of a gaseous odorant using a simple microfluidic technique. Furthermore, we verified that our system can recognize and discriminate the smell of a flower through qualitative and quantitative analyses. Based on these results, we expect our system to be used to screen gaseous odorant molecules and pattern various combinations of gaseous odorant molecules.

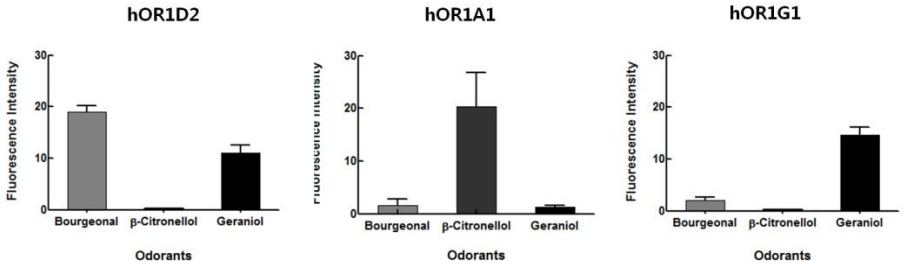

Figure 8.5 Selective response of the OR to the gaseous odorant molecules. hOR1D2, hOR1A1, and hOR1G1 were chosen and expressed in the HEK293 cells on the membrane. The ligands of the ORs (hOR1D2, hOR1A1, and hOR1G1) were known as bourgeonal, β-citronellol, and geraniol, respectively. Each OR was stimulated with 200 ppm of different gaseous odorants using a microfluidic device. Only when the OR was stimulated with its counterpart ligand was the highest fluorescence signal detected.

8.6 Conclusions

The development of the odorant detection system using artificial olfactory cell for mimicking human olfaction, have been an important topic for many years. However, the conventional systems have detected the odorant in liquid phase, so have limitation to mimic the natural olfaction system, which detect the odorant in gas phase. In this study, the odorant responses was detected and visualized in gas phase using microfluidic system and PC membrane. The cell cultured-PC membrane was placed in inverted formant in the PDMS chamber and the gaseous odorant was injected and stimulated the cells by passing the porous membrane. In this system, the gaseous odorant could reach to the expressed-cell effectively by reducing the distance between the odorant and cells. In this system, the gaseous odorant could reach to the expressed-cell effectively by reducing the distance between the odorant and cells. This system also has advantages that the odorant detection can be conducted with just small amounts of sample in the miniaturized chamber and that the chamber can be easily reused because it is not required for the cell culture in the chamber. The odorant detection was visualized using the flou-4, which is the widely used calcium indicate dye. The conventional calcium imaging system using fluo-4 has been used to detect the odorant in liquid phase; however, in this study, the calcium imaging was effectively carried out in gas phase. This system also shows good results in dose-dependent and selectivity test. This results offer the great potential that this system can be used to detect the commercially and medically meaningful odorants by mimicking the

natural olfaction system. And also can be used to study the cellular response to gaseous ligand through the signaling pathway.

Chapter 9.

Overall discussion and further suggestions

Chapter 9. Overall discussion and further suggestion

Human olfaction discriminates more than thousands of odorant molecules with high sensitivity and selectivity. About 390 ORs, which are expressed in the olfactory epithelium, play a great role to bind and detect the numerous odorants. One OR binds to various odorant with a different affinity and one odorant binds to various odorant with a different affinity. Human smell through the combination of various binding of OR and odorant. Therefore, both the characterization of the specific OR and the pattern analysis of various ORs are very important to understand the human olfaction and to apply the OR as an odorant sensing materials in various areas. And if the various odorant binding are simultaneously visualized, the effective analysis of odorant binding pattern will be possible. The visualized binding pattern also can be used as a code for specific smell.

In this thesis, various visualization methods were suggested to characterize the OR and to analyze the odorant binding pattern, combining the hOR or the cells expressing hOR and the various optical detection systems.

In chapter 4, the detection of odorant binding using SPR was presented. The hOR, which was expressed in *E. coli* system, was used as a sensing material. Because the OR is expressed in the *E. coli* system majorly as an inclusion body, it is essential to provide a proper condition for hORs to have a functional structure so that they can be used as effective sensing materials. In this chapter, the hORs, which was partially purified with detergent, was reconstituted in a liposome the lipid/detergent mixed micelle. After the

conditions to make lipid/detergent mixed micelle and liposome containing hORs were optimized, the reconstituted hOR was immobilized on the gold surface. The activity of the reconstituted hORs upon ligand stimulation was analyzed by reflectance change using SPR system. The reconstituted hOR responded to the odorant in dose-dependent manner and also selectively binds to its ligand odorant from other odorants. This study shows that the hORs, which is expressed in *E. coli*, can be used as efficient sensing material by combining with the SPR system using reconstitution process.

In chapter 5, CRE reporter assay system and the PEG microwell fabrication was optimized for visualization of odorant response of hOR in high-through manner. The vector system containing CRE reporter gene was constructed by molecular cloning, and the green fluorescence protein ZsGreen was used as a reporter protein. The HEK-293 cell line containing CRE reporter system was constructed and tested using forskolin. The expression level of the fluorescence protein was enhanced by control of the number of CRE sites and the concentration of IBMX. For the developing the miniaturized high-throughput screening platform, the PEG microwell was fabricated using PDMS stamp and PEGDA solution under UV exposure. The concentration of PEGDA solution and the UV exposure time were optimized. When the cells were seeded into the PEG microwell, each well contained 300-400 cells and the cells showed good morphology and the normal cellular activity of CRE reporter system.

In chapter 6, the PEG microwell system was combined with the reverse transfection technique for the construction of the simple and miniaturized

high-throughput odorant screening platform. The transfection mixture containing various hOR genes were spotted on the PEG microwell and the HEK-293 cells containing CRE reporter system were seeded into the PEG microwell. Various hORs were simultaneously expressed in the cells on the PEG microwell with good efficiency. This result indicates that the PEG microwell is a good barrier to prevent the cross-contamination between transfection mixtures on each well. The various OR-odorant bindings were patterned by imaging the fluorescence generated by the reporter protein under odorant stimulation and the fluorescence was calculated using software ImageJ. Also, the dose-dependent response of hOR to odorant was detected, and the EC_{50} value was 10 fold lower than the conventional calcium imaging system. This study shows that the PEG microwell-based odorant screening system is useful for the qualitative and quantitative analysis as well as for the visualization of odorant response.

In chapter 7, hOR was coupled to the potassium channel Kir6.2 by molecular cloning technique for visualizing the odorant binding pattern in real time using membrane potential dye. The various hOR-Ks were constructed and were expressed in HEK-293 cells. When the odorant binds to hOR part of hOR-K, the conformational change of hOR transmits it to the linked ion channel to open, and the potassium ion enter into the cell through the channel. The ion influx upon the odorant stimulation was imaged by fluorescence image scanner using membrane potential dye. As a result, the cells expressing hOR-K showed the higher sensitivity than the cells expressing only hOR when the odorant was added. With this method, the various odorant responses

of one hOR-K and the various odorant responses of various hOR-Ks were patterned in real time. Because the odorant binding can be detected through the conformational change of hOR as well as the intracellular signaling pathway, the hOR-K has a potential to be used as an efficient sensing material both in cell- and protein-based odorant detection system.

In chapter 8, the odorant response was visualized using microfluidic system in gas phase. The conventional calcium imaging system was conducted only in liquid phase, but, odorant detection in gas phase is important to mimic the human olfactory system and to apply in medical and industrial area. In this chapter, the odorant detection system for the detection of the well-used flowery odorant (rose and a lily of the valley) in gas phase was developed. The each transfected cells with the vector containing three different hOR genes were cultured on the polycarbonate membrane for expressing of hOR. Then, the calcium indicator flou-4 was loaded in the cells on the PC membrane and the membrane was placed in inverted format between top and bottom PDMS chamber. The gaseous odorant was injected using syringe in 1 mL/s and the odorant binding was imaged by the fluorescence of fluo-4. The cells dose-dependently responded to the odorant and the each cells expressing different hOR selectively responded to its specific odorant. The results offer a potential of the microfluidic odorant detection system as an effective tool to be used in various application area by detecting and the odorant in gas phase.

In this thesis, the high-throughput odorant visualization system was developed. The hOR protein or the artificial cells expressing hOR were used as sensing material combined with the optical detection system for the

visualization of odorant response and pattern analysis. The modification of intracellular system, modification of hOR, and various odorant detection platforms were used. Various odorant responses of various ORs were visualized effectively through the construction of the high-throughput platform, and the real time visualization of odorant response system was developed by coupling OR to the ion channel. For various applications, the response of gaseous odorant was also visualized using microfluidic system by mimicking natural human olfactory system. To visualize the odorant response, intracellular signaling and the physical conformational change of OR was used. Each cell- or protein-based visualizing system has advantages. The system using intracellular signaling of the artificial olfactory cells provide the biological information about the cellular response upon odorant stimulation. However, this cell-based system is largely dependent on the cellular condition. Thus, in this study, the simple experimental process was developed using CRE reporter assay that generates green fluorescence upon odorant stimulation. Moreover, to overcome the limitation of the cell-based system, the physical change of OR upon odorant response was also used as a protein-based system. In this system, the odorant detection can be carried out even when the environmental conditions are unfavorable to the cells. Thus, the protein-based visualizing system can be more practically used as an odorant detection system even though the system has a limitation of that it cannot provide the many of biological information about human olfaction.

Visualization of odorant response has several important meanings. First, easy and reliable characterization of orphaned OR can be conducted using the

imaging system such as fluorescence microscopy and fluorescence image scanner. Using visualization technique on the high-throughput platform, many of orphaned ORs can be characterized efficiently. Second, through the various odorant response pattern of one specific OR, the information of the OR's function can be collected by the visualized data. Third, the visualized pattern of odorant response can provide important information about human olfactory system, which recognizes the smell via the combination of various OR-odorant binding. Finally, the various smells can be discriminated and classified by the visualized pattern, thus the pattern can be used in various fields.

The odorant detection platform using various visualization techniques, which was developed in this thesis, can be used to characterize the many orphaned ORs and to analyze the binding of OR to odorants which have various molecular structures. To fully understand the human olfaction system, enough database of OR-odorant bindings should be obtained. The suggested high-throughput system using visualization technique can be used to obtain the massive amount of database by the efficient and fast odorant detection. And the database would help to construct the code for specific smell. Consequently, as this system is applied to more various ORs and odorants, the various smell patterns providing the information about the various OR-odorant bindings can be constructed, and the pattern can be used as a code for smell.

Bibliography

1. R.R. Reed, How does the nose know?, *Cell* **60** (1990) 1-2.

2. S. Firestein, How the olfactory system makes sense of scents, *Nature* **413** (2001) 211-218.

3. Y. Hasin-Brumshtein, D. Lancet, T. Olender, Human olfaction: from genomic variation to phenotypic diversity, *Trends in Genetics* **25** (2009) 178-184.

4. P. Nikitin, A. Grigorenko, A. Beloglazov, M. Valeiko, A. Savchuk, O. Savchuk, G. Steiner, C. Kuhne, A. Huebner, R. Salzer, Surface plasmon resonance interferometry for micro-array biosensing, *Sensors and Actuators A: Physical* **85** (2000) 189-193.

5. B. Malnic, J. Hirono, T. Sato, L.B. Buck, Combinatorial receptor codes for odors, *Cell* **96** (1999) 713-723.

6. K. Mori, H. Nagao, Y. Yoshihara, The olfactory bulb: coding and processing of odor molecule information, *Science* **286** (1999) 711-715.

7. L. Buck, R. Axel, A novel multigene family may encode odorant receptors: a molecular basis for odor recognition, *Cell* **65** (1991) 175-187.

8. J. Krieger, H. Breer, Olfactory reception in invertebrates, *Science* **286** (1999) 720-723.

9. F. Röck, N. Barsan, U. Weimar, Electronic nose: current status and future trends, *Chemical Reviews* **108** (2008) 705-725.

10. T.C. Pearce, J.W. Gardner, S. Friel, P.N. Bartlett, N. Blair, Electronic nose for monitoring the flavour of beers, *Analyst* **118** (1993) 371-377.

11. J.W. Gardner, H. Shurmer, T. Tan, Application of an electronic nose to the discrimination of coffees, *Sensors and Actuators B: Chemical* **6** (1992) 71-

75.

12. J.M. Vidic, J. Grosclaude, M.A. Persuy, J. Aioun, R. Salesse, E. Pajot-Augy, Quantitative assessment of olfactory receptors activity in immobilized nanosomes: a novel concept for bioelectronic nose, *Lab on a chip* **6** (2006) 1026-1032.

13. S.H. Lee, T.H. Park, Recent advances in the development of bioelectronic nose, *Biotechnology and Bioprocess Engineering* **15** (2010) 22-29.

14. Q. Liu, H. Cai, Y. Xu, Y. Li, R. Li, P. Wang, Olfactory cell-based biosensor: a first step towards a neurochip of bioelectronic nose, *Biosensors and Bioelectronics* **22** (2006) 318-322.

15. J. Pevsner, R.R. Trifiletti, S.M. Strittmatter, S.H. Snyder, Isolation and characterization of an olfactory receptor protein for odorant pyrazines, *Proceedings of the National Academy of Sciences* **82** (1985) 3050-3054.

16. O. Man, T. Olender, D. Lancet, Human Olfactory Receptors, *Handbook of Cell Signaling, Three-Volume Set* (2003) 145.

17. K.J. Ressler, S.L. Sullivan, L.B. Buck, Information coding in the olfactory system: evidence for a stereotyped and highly organized epitope map in the olfactory bulb, *Cell* **79** (1994) 1245-1255.

18. B. Malnic, P.A. Godfrey, L.B. Buck, The human olfactory receptor gene family, *Proceedings of the National Academy of Sciences of the United States of America* **101** (2004) 2584-2589.

19. H.J. Ko, T.H. Park, Enhancement of odorant detection sensitivity by the expression of odorant-binding protein, *Biosensors and Bioelectronics* **23** (2008) 1017-1023.

20. J. Pevsner, R.R. Reed, P.G. Feinstein, S.H. Snyder, Molecular cloning of odorant-binding protein: member of a ligand carrier family, *Science* **241** (1988) 336-339.

21. P. Pelosi, Odorant-binding proteins, *Critical Reviews in Biochemistry and Molecular Biology* **29** (1994) 199-228.

22. K. Touhara, Odor discrimination by G protein-coupled olfactory receptors, *Microscopy Research and Technique* **58** (2002) 135-141.

23. A.I. Farbman, *Cell biology of olfaction*1992: Cambridge University Press.

24. D.T. Jones, R.R. Reed, Golf: an olfactory neuron specific-G protein involved in odorant signal transduction, *Science* **244** (1989) 790-795.

25. K. Touhara, S. Sengoku, K. Inaki, A. Tsuboi, J. Hirono, T. Sato, H. Sakano, T. Haga, Functional identification and reconstitution of an odorant receptor in single olfactory neurons, *Proceedings of the National Academy of Sciences* **96** (1999) 4040-4045.

26. H. Breer, I. Boekhoff, Odorants of the same odor class activate different second messenger pathways, *Chemical Senses* **16** (1991) 19-29.

27. I. Boekhoff, H. Breer, Termination of second messenger signaling in olfaction, *Proceedings of the National Academy of Sciences* **89** (1992) 471-474.

28. B.W. Ache. Towards a common strategy for transducing olfactory information. in Seminars in Cell Biology. 1994. Elsevier.

29. T. Nakamura, G.H. Gold, A cyclic nucleotide-gated conductance in olfactory receptor cilia, *Nature* **325** (1987) 442-444.

30. K.J. Ressler, S.L. Sullivan, L.B. Buck, A zonal organization of odorant receptor gene expression in the olfactory epithelium, *Cell* **73** (1993) 597-609.

31. J.A. Buettner, G. Glusman, N. Ben-Arie, P. Ramos, D. Lancet, G.A. Evans, Organization and evolution of olfactory receptor genes on human chromosome 11, *Genomics* **53** (1998) 56-68.

32. G. Glusman, S. Clifton, B. Roe, D. Lancet, Sequence analysis in the olfactory receptor gene cluster on human chromosome 17: recombinatorial events affecting receptor diversity, *Genomics* **37** (1996) 147-160.

33. I. Boekhoff, E. Tareilus, J. Strotmann, H. Breer, Rapid activation of alternative second messenger pathways in olfactory cilia from rats by different odorants, *The EMBO journal* **9** (1990) 2453.

34. L.B. Buck, Information coding in the vertebrate olfactory system, *Annual Review of Neuroscience* **19** (1996) 517-544.

35. N.S. Levy, H.A. Bakalyar, R.R. Reed, Signal transduction in olfactory neurons, *The Journal of steroid biochemistry and molecular biology* **39** (1991) 633-637.

36. T. Leinders-Zufall, M.N. Rand, G.M. Shepherd, C.A. Greer, F. Zufall, Calcium entry through cyclic nucleotide-gated channels in individual cilia of olfactory receptor cells: spatiotemporal dynamics, *The Journal of Neuroscience* **17** (1997) 4136-4148.

37. K. Touhara, Deorphanizing vertebrate olfactory receptors: recent advances in odorant-response assays, *Neurochemistry International* **51** (2007) 132-139.

38. K. Schmiedeberg, E. Shirokova, H.-P. Weber, B. Schilling, W. Meyerhof, D. Krautwurst, Structural determinants of odorant recognition by the human olfactory receptors OR1A1 and OR1A2, *Journal of Structural Biology* **159** (2007) 400-412.

39. S. Katada, T. Nakagawa, H. Kataoka, K. Touhara, Odorant response assays for a heterologously expressed olfactory receptor, *Biochemical and Biophysical Research Communications* **305** (2003) 964-969.

40. H. Saito, Q. Chi, H. Zhuang, H. Matsunami, J.D. Mainland, Odor coding by a Mammalian receptor repertoire, *Science signaling* **2** (2009) ra9.

41. E. Shirokova, K. Schmiedeberg, P. Bedner, H. Niessen, K. Willecke, J.-D. Raguse, W. Meyerhof, D. Krautwurst, Identification of specific ligands for orphan olfactory receptors G protein-dependent agonism and antagonism of

odorants, *Journal of Biological Chemistry* **280** (2005) 11807-11815.

42. H. Saito, M. Kubota, R.W. Roberts, Q. Chi, H. Matsunami, RTP family members induce functional expression of mammalian odorant receptors, *Cell* **119** (2004) 679-691.

43. C. Moon, P. Jaberi, A. Otto-Bruc, W. Baehr, K. Palczewski, G.V. Ronnett, Calcium-sensitive particulate guanylyl cyclase as a modulator of cAMP in olfactory receptor neurons, *The Journal of Neuroscience* **18** (1998) 3195-3205.

44. D. Krautwurst, K.-W. Yau, R.R. Reed, Identification of ligands for olfactory receptors by functional expression of a receptor library, *Cell* **95** (1998) 917-926.

45. F. Zufall, T. Leinders-Zufall, Calcium imaging in the olfactory system: new tools for visualizing odor recognition, *The Neuroscientist* **5** (1999) 4-7.

46. U.B. Kaupp, R. Seifert, Cyclic nucleotide-gated ion channels, *Physiological Reviews* **82** (2002) 769.

47. T. Miyamoto, D. Restrepo, E.J. Cragoe Jr, J.H. Teeter, IP3-and cAMP-induced responses in isolated olfactory receptor neurons from the channel catfish, *The Journal of membrane biology* **127** (1992) 173-183.

48. Y. Okada, J.H. Teeter, D. Restrepo, Inositol 1, 4, 5-trisphosphate-gated conductance in isolated rat olfactory neurons, *Journal of Neurophysiology* **71** (1994) 595-602.

49. G. Levasseur, M.-A. Persuy, D. Grebert, J.-J. Remy, R. Salesse, E. Pajot-Augy, Ligand-specific dose–response of heterologously expressed olfactory receptors, *European Journal of Biochemistry* **270** (2003) 2905-2912.

50. K. Kajiya, K. Inaki, M. Tanaka, T. Haga, H. Kataoka, K. Touhara, Molecular bases of odor discrimination: reconstitution of olfactory receptors that recognize overlapping sets of odorants, *The Journal of Neuroscience* **21** (2001) 6018-6025.

51. C.H. Wetzel, M. Oles, C. Wellerdieck, M. Kuczkowiak, G. Gisselmann, H. Hatt, Specificity and sensitivity of a human olfactory receptor functionally expressed in human embryonic kidney 293 cells and Xenopus laevis oocytes, *The Journal of Neuroscience* **19** (1999) 7426-7433.

52. H. Hatt, G. Gisselmann, C. Wetzel, Cloning, functional expression and characterization of a human olfactory receptor, *Cellular and molecular biology (Noisy-le-Grand, France)* **45** (1999) 285-291.

53. M. Spehr, G. Gisselmann, A. Poplawski, J.A. Riffell, C.H. Wetzel, R.K. Zimmer, H. Hatt, Identification of a testicular odorant receptor mediating human sperm chemotaxis, *Science* **299** (2003) 2054-2058.

54. E.M. Neuhaus, A. Mashukova, W. Zhang, J. Barbour, H. Hatt, A specific heat shock protein enhances the expression of mammalian olfactory receptor proteins, *Chemical Senses* **31** (2006) 445-452.

55. G. Sanz, C. Schlegel, J.-C. Pernollet, L. Briand, Comparison of odorant specificity of two human olfactory receptors from different phylogenetic classes and evidence for antagonism, *Chemical Senses* **30** (2005) 69-80.

56. V. Matarazzo, O. Clot-Faybesse, B. Marcet, G. Guiraudie-Capraz, B. Atanasova, G. Devauchelle, M. Cerutti, P. Etiévant, C. Ronin, Functional characterization of two human olfactory receptors expressed in the baculovirus Sf9 insect cell system, *Chemical Senses* **30** (2005) 195-207.

57. C. Moon, Y.-K. Sung, R. Reddy, G.V. Ronnett, Odorants induce the phosphorylation of the cAMP response element binding protein in olfactory receptor neurons, *Proceedings of the National Academy of Sciences* **96** (1999) 14605-14610.

58. Q. Shan, D.R. Storm, Optimization of a cAMP response element signal pathway reporter system, *Journal of Neuroscience Methods* **191** (2010) 21-25.

59. S.J. Hill, J.G. Baker, S. Rees, Reporter-gene systems for the study of G-protein-coupled receptors, *Current Opinion in Pharmacology* **1** (2001) 526-532.

60. Y. Fujita, T. Takahashi, A. Suzuki, K. Kawashima, F. Nara, R. Koishi, Deorphanization of Dresden G protein-coupled receptor for an odorant receptor, *Journal of Receptors and Signal Transduction* **27** (2007) 323-334.

61. Y. Takeuchi, K. Fukunaga, Differential regulation of NF-κB, SRE and CRE by dopamine D1 and D2 receptors in transfected NG108-15 cells, *Journal of Neurochemistry* **85** (2003) 729-739.

62. H. Zhuang, H. Matsunami, Synergism of accessory factors in functional expression of mammalian odorant receptors, *Journal of Biological Chemistry* **282** (2007) 15284-15893.

63. H. Dacres, J. Wang, V. Leitch, I. Horne, A.R. Anderson, S.C. Trowell, Greatly enhanced detection of a volatile ligand at femtomolar levels using bioluminescence resonance energy transfer (BRET), *Biosensors and Bioelectronics* **29** (2011) 119-124.

64. A. Mashukova, M. Spehr, H. Hatt, E.M. Neuhaus, β-arrestin2-mediated internalization of mammalian odorant receptors, *The Journal of Neuroscience* **26** (2006) 9902-9912.

65. E.H. Oh, H.S. Song, T.H. Park, Recent advances in electronic and bioelectronic noses and their biomedical applications, *Enzyme and Microbial Technology* **48** (2011) 427-437.

66. Q. Liu, W. Ye, L. Xiao, L. Du, N. Hu, P. Wang, Extracellular potentials recording in intact olfactory epithelium by microelectrode array for a bioelectronic nose, *Biosensors and Bioelectronics* **25** (2010) 2212-2217.

67. E. Micholt, D. Jans, G. Callewaert, C. Bartic, J. Lammertyn, B. Nicolaï, Extracellular recordings from rat olfactory epithelium slices using micro electrode arrays, *Sensors and Actuators B: Chemical* **184** (2013) 40-47.

68. K. Chen, H. Obinata, T. Izumi, Detection of G protein-coupled receptor-mediated cellular response involved in cytoskeletal rearrangement using surface plasmon resonance, *Biosensors and Bioelectronics* **25** (2010) 1675-1680.

69. V. Jacquier, H. Pick, H. Vogel, Characterization of an extended receptive ligand repertoire of the human olfactory receptor OR17- 40 comprising structurally related compounds, *Journal of Neurochemistry* **97** (2006) 537-544.

70. J.H. Sung, H.J. Ko, T.H. Park, Piezoelectric biosensor using olfactory receptor protein expressed in *Escherichia coli*, *Biosensors and Bioelectronics* **21** (2006) 1981-1986.

71. H.J. Ko, T.H. Park, Piezoelectric olfactory biosensor: ligand specificity and dose-dependence of an olfactory receptor expressed in a heterologous cell system, *Biosensors and Bioelectronics* **20** (2005) 1327-1332.

72. T.H. Kim, S.H. Lee, J. Lee, H.S. Song, E.H. Oh, T.H. Park, S. Hong, Single-carbon-atomic-resolution detection of odorant molecules using a human olfactory receptor-based bioelectronic Nose, *Advanced Materials* **21** (2009) 91-94.

73. B. Ding, M. Wang, J. Yu, G. Sun, Gas sensors based on electrospun nanofibers, *Sensors* **9** (2009) 1609-1624.

74. E. Dalcanale, J. Hartmann, Selective detection of organic compounds by means of cavitand-coated QCM transducers, *Sensors and Actuators B: Chemical* **24** (1995) 39-42.

75. R. Lucklum, P. Hauptmann, The quartz crystal microbalance: mass sensitivity, viscoelasticity and acoustic amplification, *Sensors and Actuators B: Chemical* **70** (2000) 30-36.

76. I.A. Koshets, Z.I. Kazantseva, Y.M. Shirshov, S.A. Cherenok, V.I. Kalchenko, Calixarene films as sensitive coatings for QCM-based gas sensors, *Sensors and Actuators B: Chemical* **106** (2005) 177-181.

77. B. Wyszynski, P. Somboon, T. Nakamoto, Pegylated lipids as coatings for QCM odor-sensors, *Sensors and Actuators B: Chemical* **121** (2007) 538-544.

78. S. Panigrahi, S. Sankaran, S. Mallik, B. Gaddam, A.A. Hanson, Olfactory

receptor-based polypeptide sensor for acetic acid VOC detection, *Materials Science and Engineering: C* **32** (2012) 1307-1313.

79. P.J. Harding, T.C. Hadingham, J.M. McDonnell, A. Watts, Direct analysis of a GPCR-agonist interaction by surface plasmon resonance, *European Biophysics Journal* **35** (2006) 709-712.

80. A. Szabo, L. Stolz, R. Granzow, Surface plasmon resonance and its use in biomolecular interaction analysis (BIA), *Current Opinion in Structural Biology* **5** (1995) 699-705.

81. I. Lundström, Real-time biospecific interaction analysis, *Biosensors and Bioelectronics* **9** (1994) 725-736.

82. B. Liedberg, C. Nylander, I. Lundström, Biosensing with surface plasmon resonance — how it all started, *Biosensors and Bioelectronics* **10** (1995) 1-6.

83. J. Homola, S.S. Yee, G. Gauglitz, Surface plasmon resonance sensors: review, *Sensors and Actuators B: Chemical* **54** (1999) 3-15.

84. I. Alves, C. Park, V. Hruby, Plasmon resonance methods in GPCR signaling and other membrane events, *Current Protein and Peptide Science* **6** (2005) 293-312.

85. L.G. Fägerstam, Å. Frostell-Karlsson, R. Karlsson, B. Persson, I. Rönnberg, Biospecific interaction analysis using surface plasmon resonance detection applied to kinetic, binding site and concentration analysis, *Journal of Chromatography A* **597** (1992) 397-410.

86. I. Navratilova, J. Besnard, A.L. Hopkins, Screening for GPCR ligands using surface plasmon resonance, *ACS Medicinal Chemistry Letters* **2** (2011) 549-554.

87. I. Benilova, V.I. Chegel, Y.V. Ushenin, J. Vidic, A.P. Soldatkin, C. Martelet, E. Pajot, N. Jaffrezic-Renault, Stimulation of human olfactory receptor 17-40 with odorants probed by surface plasmon resonance, *European Biophysics Journal* **37** (2008) 807-814.

88. S.H. Lee, H.J. Ko, T.H. Park, Real-time monitoring of odorant-induced cellular reactions using surface plasmon resonance, *Biosensors and Bioelectronics* **25** (2009) 55-60.

89. J.Y. Lee, H.J. Ko, S.H. Lee, T.H. Park, Cell-based measurement of odorant molecules using surface plasmon resonance, *Enzyme and Microbial Technology* **39** (2006) 375-380.

90. J. Vidic, M. Pla-Roca, J. Grosclaude, M.-A. Persuy, R. Monnerie, D. Caballero, A. Errachid, Y. Hou, N. Jaffrezic-Renault, R. Salesse, Gold surface functionalization and patterning for specific immobilization of olfactory receptors carried by nanosomes, *Analytical Chemistry* **79** (2007) 3280-3290.

91. J. Vidic, J. Grosclaude, R. Monnerie, M.-A. Persuy, K. Badonnel, C. Baly, M. Caillol, L. Briand, R. Salesse, E. Pajot-Augy, On a chip demonstration of a functional role for odorant binding protein in the preservation of olfactory receptor activity at high odorant concentration, *Lab on a chip* **8** (2008) 678-688.

92. H.J. Ko, S.H. Lee, E.H. Oh, T.H. Park, Specificity of odorant-binding proteins: a factor influencing the sensitivity of olfactory receptor-based biosensors, *Bioprocess and Biosystems Engineering* **33** (2010) 55-62.

93. G. Gomila, I. Casuso, A. Errachid, O. Ruiz, E. Pajot, J. Minic, T. Gorojankina, M. Persuy, J. Aioun, R. Salesse, Advances in the production, immobilization, and electrical characterization of olfactory receptors for olfactory nanobiosensor development, *Sensors and Actuators B: Chemical* **116** (2006) 66-71.

94. I.V. Benilova, J. Minic Vidic, E. Pajot-Augy, A.P. Soldatkin, C. Martelet, N. Jaffrezic-Renault, Electrochemical study of human olfactory receptor OR 17–40 stimulation by odorants in solution, *Materials Science and Engineering: C* **28** (2008) 633-639.

95. Y. Hou, N. Jaffrezic-Renault, C. Martelet, A. Zhang, J. Minic-Vidic, T. Gorojankina, M.-A. Persuy, E. Pajot-Augy, R. Salesse, V. Akimov, A novel detection strategy for odorant molecules based on controlled bioengineering of rat olfactory receptor I7, *Biosensors and Bioelectronics* **22** (2007) 1550-

1555.

96. S.H. Lee, S.B. Jun, H.J. Ko, S.J. Kim, T.H. Park, Cell-based olfactory biosensor using microfabricated planar electrode, *Biosensors and Bioelectronics* **24** (2009) 2659-2664.

97. S.H. Lee, S.H. Jeong, S.B. Jun, S.J. Kim, T.H. Park, Enhancement of cellular olfactory signal by electrical stimulation, *Electrophoresis* **30** (2009) 3283-3288.

98. H.J. Jin, S.H. Lee, T.H. Kim, J. Park, H.S. Song, T.H. Park, S. Hong, Nanovesicle-based bioelectronic nose platform mimicking human olfactory signal transduction, *Biosensors and Bioelectronics* **35** (2012) 335-341.

99. J.H. Lim, J. Park, E.H. Oh, H.J. Ko, S. Hong, T.H. Park, Nanovesicle-Based Bioelectronic Nose for the Diagnosis of Lung Cancer from Human Blood, *Advanced Healthcare Materials* (2013)

100. J.H. Lim, J. Park, J.H. Ahn, H.J. Jin, S. Hong, T.H. Park, A peptide receptor-based bioelectronic nose for the real-time determination of seafood quality, *Biosensors and Bioelectronics* **39** (2012) 244-249.

101. H. Yoon, S.H. Lee, O.S. Kwon, H.S. Song, E.H. Oh, T.H. Park, J. Jang, Polypyrrole nanotubes conjugated with human olfactory receptors: high-performance transducers for FET-type bioelectronic noses, *Angewandte Chemie International Edition* **48** (2009) 2755-2758.

102. S.H. Lee, O.S. Kwon, H.S. Song, S.J. Park, J.H. Sung, J. Jang, T.H. Park, Mimicking the human smell sensing mechanism with an artificial nose platform, *Biomaterials* **33** (2012) 1722-1729.

103. N.A. Rakow, K.S. Suslick, A colorimetric sensor array for odour visualization, *Nature* **406** (2000) 710-713.

104. V. Jacquier, M. Prummer, J.-M. Segura, H. Pick, H. Vogel, Visualizing odorant receptor trafficking in living cells down to the single-molecule level, *Proceedings of the National Academy of Sciences* **103** (2006) 14325-14330.

105. X.A. Figueroa, G.A. Cooksey, S.V. Votaw, L.F. Horowitz, A. Folch, Large-

scale investigation of the olfactory receptor space using a microfluidic microwell array, *Lab on a chip* **10** (2010) 1120-1127.

106. T.M. Redmond, X. Ren, G. Kubish, S. Atkins, S. Low, M.D. Uhler, Microarray transfection analysis of transcriptional regulation by cAMP-dependent protein kinase, *Molecular & Cellular Proteomics* **3** (2004) 770-779.

107. C.J. Moreau, J.P. Dupuis, J. Revilloud, K. Arumugam, M. Vivaudou, Coupling ion channels to receptors for biomolecule sensing, *Nature Nanotechnology* **3** (2008) 620-625.

108. H. Zhao, L. Ivic, J.M. Otaki, M. Hashimoto, K. Mikoshiba, S. Firestein, Functional expression of a mammalian odorant receptor, *Science* **279** (1998) 237-242.

109. J. Minic, M.A. Persuy, E. Godel, J. Aioun, I. Connerton, R. Salesse, E. Pajot- Augy, Functional expression of olfactory receptors in yeast and development of a bioassay for odorant screening, *FEBS Journal* **272** (2005) 524-537.

110. H.J. Ko, T. Hyun Park, Dual signal transduction mediated by a single type of olfactory receptor expressed in a heterologous system, *Biological Chemistry* **387** (2006) 59-68.

111. C. Hague, M.A. Uberti, Z. Chen, C.F. Bush, S.V. Jones, K.J. Ressler, R.A. Hall, K.P. Minneman, Olfactory receptor surface expression is driven by association with the β2-adrenergic receptor, *Proceedings of the National Academy of Sciences of the United States of America* **101** (2004) 13672-13676.

112. J.H. Dunham, R.A. Hall, Enhancement of the surface expression of G protein-coupled receptors, *Trends in Biotechnology* **27** (2009) 541-545.

113. P. Stenlund, G.J. Babcock, J. Sodroski, D.G. Myszka, Capture and reconstitution of G protein-coupled receptors on a biosensor surface, *Analytical Biochemistry* **316** (2003) 243-250.

114. S.G. Patching, Surface plasmon resonance spectroscopy for characterisation of membrane protein–ligand interactions and its potential for drug discovery, *Biochimica et Biophysica Acta (BBA)-Biomembranes* **1838** (2014) 43-55.

115. H.S. Song, S.H. Lee, E.H. Oh, T.H. Park, Expression, solubilization and purification of a human olfactory receptor from *Escherichia coli*, *Current Microbiology* **59** (2009) 309-314.

116. T. Mirzabekov, H. Kontos, M. Farzan, W. Marasco, J. Sodroski, Paramagnetic proteoliposomes containing a pure, native, and oriented seven-transmembrane segment protein, CCR5, *Nature Biotechnology* **18** (2000) 649-654.

117. K. Glasmästar, C. Larsson, F. Höök, B. Kasemo, Protein adsorption on supported phospholipid bilayers, *Journal of Colloid and Interface Science* **246** (2002) 40-47.

118. M. Beseničar, P. Maček, J.H. Lakey, G. Anderluh, Surface plasmon resonance in protein–membrane interactions, *Chemistry and Physics of Lipids* **141** (2006) 169-178.

119. L.V. Galietta, S. Jayaraman, A. Verkman, Cell-based assay for high-throughput quantitative screening of CFTR chloride transport agonists, *American Journal of Physiology-Cell Physiology* **281** (2001) C1734-C1742.

120. B.L. Apostol, A. Kazantsev, S. Raffioni, K. Illes, J. Pallos, L. Bodai, N. Slepko, J.E. Bear, F.B. Gertler, S. Hersch, A cell-based assay for aggregation inhibitors as therapeutics of polyglutamine-repeat disease and validation in Drosophila, *Proceedings of the National Academy of Sciences of the United States of America* **100** (2003) 5950-5955.

121. S.A. Sundberg, High-throughput and ultra-high-throughput screening: solution-and cell-based approaches, *Current Opinion in Biotechnology* **11** (2000) 47-53.

122. Y.-X. Yan, D.M. Boldt-Houle, B.P. Tillotson, M.A. Gee, J. Brian, X.-J. Chang, C.E. Olesen, M.A. Palmer, Cell-based high-throughput screening assay system for monitoring G protein-coupled receptor activation using β-galactosidase enzyme complementation technology, *Journal of Biomolecular*

Screening **7** (2002) 451-459.

123. J. Ziauddin, D.M. Sabatini, Microarrays of cells expressing defined cDNAs, *Nature* **411** (2001) 107-110.

124. Y.M. Mishina, C.J. Wilson, L. Bruett, J.J. Smith, C. Stoop-Myer, S. Jong, L.P. Amaral, R. Pedersen, S.K. Lyman, V.E. Myer, Multiplex GPCR assay in reverse transfection cell microarrays, *Journal of Biomolecular Screening* **9** (2004) 196-207.

125. M. Sturzl, A. Konrad, G. Sander, E. Wies, F. Neipel, E. Naschberger, S. Reipschlager, N. Gonin-Laurent, R.E. Horch, U. Kneser, High throughput screening of gene functions in mammalian cells using reversely transfected cell arrays: review and protocol, *Combinatorial Chemistry and High Throughput Screening* **11** (2008) 159-172.

126. D. Castel, A. Pitaval, M.A. Debily, X. Gidrol, Cell microarrays in drug discovery, *Drug Discovery Today* **11** (2006) 616-622.

127. E. Hodges, J.S. Redelius, W. Wu, C. Höög, Accelerated discovery of novel protein function in cultured human cells, *Molecular & Cellular Proteomics* **4** (2005) 1319-1327.

128. T. Peterbauer, J. Heitz, M. Olbrich, S. Hering, Simple and versatile methods for the fabrication of arrays of live mammalian cells, *Lab on a chip* **6** (2006) 857-863.

129. C.H. Kwon, I.R. Wheeldon, N.N. Kachouie, S. Lee, H. Bae, S. Sant, J. Fukuda, J.W. Kang, A. Khademhosseini, Drug-eluting microarrays for cell-based screening of chemical-induced apoptosis, *Analytical Chemistry* **83** (2011) 4118-4125.

130. H.C. Moeller, M.K. Mian, S. Shrivastava, B.G. Chung, A. Khademhosseini, A microwell array system for stem cell culture, *Biomaterials* **29** (2008) 752-763.

131. S.A. Kobel, M.P. Lutolf, Fabrication of PEG hydrogel microwell arrays for high-throughput single stem cell culture and analysis, in Nanotechnology in

Regenerative Medicine2012, Springer. p. 101-112.

132. Y.Y. Choi, B.G. Chung, D.H. Lee, A. Khademhosseini, J.-H. Kim, S.-H. Lee, Controlled-size embryoid body formation in concave microwell arrays, *Biomaterials* **31** (2010) 4296-4303.

133. M. Charnley, M. Textor, A. Khademhosseini, M.P. Lutolf, Integration column: microwell arrays for mammalian cell culture, *Integrative Biology* **1** (2009) 625-634.

134. K. Knape, A. Beyer, A. Stary, G. Buchbauer, P. Wolschann, Evolutionary trace of human odorant receptors of chromosome 17, *FLAVOUR AND FRAGRANCE JOURNAL* **24** (2009) 192-197.

135. V. Jacquier, H. Pick, H. Vogel, Characterization of an extended receptive ligand repertoire of the human olfactory receptor OR17-40 comprising structurally related compounds, *Journal of Neurochemistry* **97** (2006) 537-544.

136. S. Haider, J.F. Antcliff, P. Proks, M.S. Sansom, F.M. Ashcroft, Focus on Kir6. 2: a key component of the ATP-sensitive potassium channel, *Journal of Molecular and Cellular Cardiology* **38** (2005) 927-936.

137. C.G. Nichols, KATP channels as molecular sensors of cellular metabolism, *Nature* **440** (2006) 470-476.

초 록

인간의 후각 시스템은 수천 가지의 냄새물질을 매우 낮은 농도까지 감지 및 구별할 수 있다. 냄새의 감지는 비강 후면의 후각 상피에 다수 포진하는 섬모 표면의 후각 수용체가 냄새 물질을 인지하는 데서 시작된다. 인간의 후각 수용체는 390여 가지에 달하며, 하나의 후각 신경세포가 하나의 후각 수용체를 발현하는 것으로 알려져 있다. 후각 수용체가 냄새분자와 결합하면 후각 수용체의 구조 변화가 일어나고, 여기서 비롯된 세포 내 신호 전달 기작에 의해 발생한 전기생리학적 신호가 뇌로 전달된다. 한 가지의 후각 수용체 단백질은 여러 종류의 냄새분자와 결합할 수 있고, 또한 한 가지의 냄새 분자는 여러 가지의 후각 수용체와 결합할 수 있는데, 인간은 후각 수용체와 냄새 분자간의 다양한 결합 패턴을 통하여 냄새를 구별하게 된다. 따라서 후각 수용체와 냄새 분자의 결합 패턴에 관련된 데이터 확보는 인간이 냄새를 인지하는 방식을 이해하기 위해 매우 중요하다. 후각 수용체의 기능을 밝히기 위해 전 세계의 많은 연구자들이 칼슘 이미징 및 CRE 리포터 어세이 등 인공 후각세포 기반의 스크리닝 시스템을 개발해 왔다. 하지만 많은 단계를 거쳐야 하는 스크리닝 실험의 특성상 대부분의 후각 수용체의 기능은 여전히 밝혀지지 않고 있는 상태이다.

본 연구에서는 후각 수용체와 냄새 분자간의 결합을 광학적 측정 기술을 활용하여 시각화함으로써 후각 수용체의 기능 및 냄새물질과의 반응 패턴을 분석하는 시스템을 개발하였다. 후각 수용체 단백질이 포함된 인공 후각세포를 냄새 측정 시스템의 1차 변환기로

활용하였고, 표면 플라즈몬 공명 (SPR) 장비, 형광 현미경, 형광 이미지 스캐너 등을 2차 변환기로 활용하였다. 후각 수용체 단백질은 대장균 발현 시스템을 통해 대량으로 확보하였고, 정제 및 리폴딩 과정을 거쳐 SPR 기반의 냄새 측정 시스템에서 1차 변환기로 이용하였다. 또한 고속 대량 스크리닝 시스템 및 냄새 측정 시스템의 시각화를 위하여 인공 후각세포를 소자로 활용하였다. 소형화된 플랫폼을 제작하기 위하여 Polyethylene glycol (PEG) 마이크로웰을 제작하였고, 역 형질주입 기술을 도입하여 다양한 후각 수용체를 마이크로웰 상에서 동시에 발현시킴으로써 고속 대량 스크리닝이 가능하도록 하였다. 또한 세포 내 신호 전달 기작을 조작하여 냄새 분자가 후각 수용체에 결합하면 녹색 형광 단백질이 발현되어 형광 현미경으로 측정 가능하도록 함으로써 냄새 반응을 시각화하였다. 기존에 널리 이용되어 온 칼슘 이미징 방법은 후각 수용체를 한 종류씩 세포에서 발현시켜야 하고 칼슘 측정용 염색약을 세포 내에 주입하여 냄새를 측정하기 때문에 대량 스크리닝이 용이하지 않았던 반면, 본 연구는 다양한 후각 수용체의 동시 발현 및 형광 단백질을 활용한 시각화로 인해 안정적인 냄새 측정 및 고속 대량 스크리닝이 가능하다는 장점이 있다. 하지만, 형광 단백질을 통해 냄새 측정이 이루어지기 때문에 단백질 발현 시간이 소요된다는 단점이 있는데, 이를 극복하기 위하여 후각 수용체의 구조 변화를 이용하여 실시간으로 냄새를 측정 및시각화하는 연구를 진행하였다.

실시간으로 냄새를 측정하기 위하여, 후각 수용체와 칼륨 이온 채널을 연결하여 후각 수용체가 냄새 분자와 결합했을 때 발생하는 구조적 변화로 인해 칼륨 이온 채널이 물리적으로 열리도록 하였다.

열린 칼륨 이온 채널을 통해 유입된 칼륨 이온을 막전위 측정용 염색약를 이용하여 측정함으로써 실시간 이미징이 가능하게 되었다. 이온 채널이 연결된 후각 수용체를 냄새 측정 시스템의 소자로 활용하게 되면 세포 내 신호 전달 기작에만 의존하던 기존 연구 방식으로부터 벗어나 후각 수용체의 구조적 변화를 이용할 수 있기 때문에, 세포의 상태가 야기하는 불안정성으로부터 자유로울 수 있다. 본 연구에서는 여러 후각 수용체 단백질들을 이온채널과 연결하여 냄새를 실시간으로 측정하고 이미징하는 냄새 측정 시스템을 개발함으로써 다양한 냄새의 패턴을 시각화하였다.

냄새 측정 시스템의 광범위한 활용을 위해서는 기체 상태의 냄새 물질을 측정하는 것이 중요하다. 따라서 본 연구에서는 마이크로플루이딕 시스템과 polycarbonate (PC) 멤브레인을 활용하여 기체 상태의 냄새 분자와 후각 수용체의 반응을 시각화하는 연구를 수행하였다. PC 멤브레인에 인공 후각세포를 배양하여 마이크로 플루이딕 시스템에 거꾸로 삽입한 후, 멤브레인 상부에 기체상태의 냄새 분자를 주입함으로써 멤브레인을 통과한 냄새 분자가 후각 수용체와 결합하여 신호를 발생시키도록 설계하였으며, 발생된 신호는 칼슘 이미징을 통해 시각화하였다.

본 연구에서는 후각 수용체와 냄새 분자의 결합 패턴을 다양한 플랫폼과 측정 기법을 활용하여 시각화하였고, 고속 대량 스크리닝 시스템 및 패턴 분석 도구로써의 활용 가능성을 제시하였다. 냄새 반응의 시각화 기술은 인간이 인지하는 냄새의 패턴을 제시할 수 있으며, 냄새에 코드를 부여하여 표준화하는 연구에 활용될 것으로 기대한다.